# IMMOBILIZED MEDIATOR ELECTRODES FOR MICROBIAL FUEL CELLS

A Thesis Submitted to the College of

Graduate Studies and Research

In Partial Fulfillment of the Requirements

For the Degree of Master of Science in the

Department of Chemical and Biological Engineering

University of Saskatchewan

Saskatoon

By

Jonathan Godwin

## PERMISSION TO USE

In presenting this thesis in partial fulfilment of the requirements for a Postgraduate degree from the University of Saskatchewan, I agree that the Libraries of this University may make it freely available for inspection. I further agree that permission for copying of this thesis in any manner, in whole or in part, for scholarly purposes may be granted by Dr. Richard Evitts who supervised my thesis work or, in his absence, by the Head of the Department or the Dean of the College of Engineering. It is understood that any copying or publication or use of this thesis or parts thereof for financial gain shall not be allowed without my written permission. It is also understood that due recognition shall be given to me and to the University of Saskatchewan in any scholarly use which may be made of any material in my thesis.

Requests for permission to copy or to make other use of material in this thesis in whole or part should be addressed to:

Head of the Department of Chemical and Biological Engineering

University of Saskatchewan

Saskatoon, Saskatchewan S7N 5A9

Canada

## ABSTRACT

With the current interest in alternative methods of energy production and increased utilization of existing energy sources, microbial fuel cells have become an important field of research. Microbial fuel cells are devices which harvest electrons from microorganisms created by their enzymatic oxidation of complex carbon substrates or consumed by their reduction of chemical oxidants. Microbial fuel cells with photosynthetic biocathodes are of particular interest due to their ability to simultaneously produce electricity and hydrocarbons while reducing carbon dioxide.

Most species of microorganisms including many bacteria and yeasts require exogenous electron transfer mediators in order to allow electron transfer with an electrode. While adding such chemicals is simple enough at a lab scale, problems arise with chemical costs and separation at a larger scale. The goal of this research was to develop electrodes composed of a robust material which will eliminate the need for added soluble electron mediators in a photosynthetic biocathode microbial fuel cell.

Electrodes made from stainless steel 304L have been coated in a conductive polymer (polypyrrole) and an immobilized electron transfer mediator (methylene blue) and tested chemically for stability and in a microbial fuel cell environment for use in bioanodes and biocathodes. The use of these immobilized mediator in the photosynthetic biocathode increased the open circuit voltage of the cell from 0.17 V to 0.24 V and the short circuit current from 8 $mA/m^2$ to 64 $mA/m^2$ (normalized to the geometric surface area of the electrode) when compared to using the same mediator in solution. The opposite effect was seen when using the electrodes in a bioanode utilizing *Saccharomyces cerevisiae*. The open circuit voltage decreased from 0.37

V to 0.31 V and the short circuit current decreased from 94 $mA/m^2$ to 24 $mA/m^2$ when comparing the immobilized mediator to soluble mediators. The impact of the membrane and pH of the anode and cathode solutions were quantified and were found to have much less of an effect on the internal resistance than the microbial factors.

## ACKNOWLEDGMENTS

I would like to express my thanks to my supervisor, Dr. Richard Evitts, for his continuous interest and support throughout my Masters work. He provided valuable advice and support for all of my ideas and experiments. I would like to thank my advisory committee, Dr. Mehdi Nemati and Dr. Aaron Phoenix, for steering my research in the right direction and pointing out some of the important issues with my work. Also, to the Natural Sciences and Engineering Research Council of Canada for their financial support of the project.

Additionally, I would like to thank Dr. Gordon Hill for his initial interest in this project, without which it probably never would have gone anywhere. I would also like to thank the Engineering staff who helped me obtain materials and build my experimental equipment.

I would like to acknowledge the help and friendship of fellow graduate students who have assisted me in research and in classes: Glyn Kennell, Jeff Huang, and Lyman Moreno. Finally, I would like to thank my parents for their support these last few years.

# TABLE OF CONTENTS


1. Introduction ..... 1

2. Background ..... 4

2.1 Microbial Fuel Cells ..... 4

2.1.1 Types of Microbial Fuel Cells ..... 5

2.1.2 Substrates and Potentials ..... 6

2.1.3 Biocathodes ..... 7

2.1.4 Photosynthetic Cathodes and Growth Rates ..... 8

2.2 MFC Electrodes ..... 9

2.3 Polymerized Redox Dyes ..... 12

2.4 Polypyrrole/salicylate ..... 13

2.5 Electrochemical Impedance Spectroscopy ..... 15

2.6 Microbial Fuel Cell Analysis and Modelling ..... 18

2.6.1 Components of microbial fuel cell resistances ..... 19

2.6.2 Electrochemical Techniques ..... 20

2.6.3 Polarization and Power Curves ..... 22

2.6.4 Modelling ..... 23

2.7 Detailed Objectives ..... 25

3. Experimental ..... 27

3.1 Equipment ..... 27

3.2 Methylene Blue Polymerization ..... 27

3.3 Stainless steel electrode preparation ..... 29

3.4 Polypyrrole synthesis ..... 29

3.5 Composite electrodes and microbial fuel cell electrode preparation ..... 30

3.6 EIS analysis of electrode coatings ..... 32
3.7 NADH catalysis measurement ..... 32
3.8 Algae culture for microbial fuel cell biocathodes ..... 33
3.9 Yeast Growth and Microbial Fuel Cell Bioanode ..... 35
3.10 Microbial Fuel Cell Analysis Procedures ..... 36
3.10.1 Cell Growth and Biomass Concentraitons ..... 37
3.10.2 Open Circuit Voltages ..... 37
3.10.3 Measuring and Plotting Polarization Curves ..... 37
3.10.4 Measuring Internal Resistances ..... 38
4. Results and Discussion ..... 39
4.1 Formation and Evaluation of Metal-based Immobilized Mediator Electrodes ..... 39
4.1.1 Conductive Polypyrrole Used to Block Oxidation of Metal Surfaces ..... 40
4.1.2 Formation of Conductive Polypyrrole on Base Metal Alloys ..... 41
4.1.3 Formation of Poly(methylene blue) on Polypyrrole Coated Steel ..... 45
4.1.4 Measurement of Film Impedance and its use in Evaluating Film Performance ..... 48
4.1.5 Degradation of Films in Aqueous Solutions ..... 50
4.1.6 Comparison of the Use of Different Doping Ions in Polypyrrole ..... 51
4.1.7 NADH Oxidation as a Method of Confirming Bioelectrochemical Activity ..... 52
4.2 Photosynthetic Biocathodes with Immobilized Mediator Electrodes ..... 54
4.2.1 Microbial Fuel Cell Operation ..... 54
4.2.2 Biocathode Open Circuit Potentials ..... 55
4.2.3 $CO_2$ Effect ..... 56
4.2.4 Transient responses to step changes ..... 57
4.2.5 Measuring Voltage-Current Relationships and Performance ..... 59
4.2.6 Comparisons to other values in literature ..... 61

4.2.7 Measuring experimental uncertainty in polarization curves ..... 61
4.3 Microbial Fuel Cell with Coupled Bioanode and Biocathode ..... 63
4.3.1 Open Circuit Voltages of Coupled MFC ..... 65
4.3.2 Summary of Different Electrodes Used in the MFC ..... 66
4.3.3 Model Fitting to Polarization Curve Data ..... 66
4.3.4 Evaluation of Anode and Cathode using Reference Electrodes ..... 67
4.3.5 Internal Resistance Components ..... 68
5. Conclusions and Recommendations ..... 71
5.1 Conclusions ..... 71
5.2 Recommendations ..... 72
References ..... 74
Appendix A. Calculation of Theoretical Potentials ..... 80

# LIST OF TABLES

Table 2.1. Half cell potentials of several substances used in microbial fuel cells calculated at standard conditions and at common microbial fuel cell conditions. [a](Logan, 2006). ..... 7

Table 3.1. Bold's Basic medium nutrients and minerals. ..... 33

Table 3.2. Yeast substrate used for bioanode studies. ..... 35

Table 4.1. Success of different anions as the counter ion during pyrrole polymerization. ..... 42

Table 4.2. Pyrrole solution used for polymerization on stainless steel. ..... 44

Table 4.3. Methylene blue synthesis solution composition. ..... 46

Table 4.4. Performance of different types of biocathodes reported in literature. ..... 61

# LIST OF FIGURES

Figure 2.1. Structure of polymerized methylene blue proposed by Karyakin (1999) with monomers joined at their nitrogen groups. ..... 13

Figure 2.2. Structure of oxidized (conductive) polypyrrole doped with an anion denoted by $A^-$. The polymer has a net charge of +1 for every three monomer units with partial positive charges on the nitrogen groups. Figure reproduced based on Vernitskaya et al. (1997)..... 15

Figure 2.3. Diagram of a microbial fuel cell with a yeast bioanode and algae biocathode. A represents algae cells, Y represents yeast cells with superscripts 'R' representing the reduced state for those cells. S is the yeast substrate (glucose) and M is the mediator compound, either attached to the electrode or in solution depending on the experiment. ..... 26

Figure 3.1. Microbial fuel cell electrode preparation cell. A graphite rod (a) is used as the counter electrode, stainless steel (b) as the working electrode onto which the polymer layers are deposited, and a saturated calomel (c) reference. ..... 31

Figure 3.2. Microbial fuel cell apparatus showing the anode (a), cathode (b), working electrode (c), reference electrode (d), Nafion-112 membrane (e), and $CO_2$ bubbler (f). ..... 36

Figure 4.1. Expected electron transfer mechanism between microbial cells and composite immobilized mediator electrode with polypyrrole and poly(methylene blue). ..... 40

Figure 4.2. Chronopotentiometry plots for deposition of polypyrrole on stainless steel 304L from solutions of different pH (shown as labels). At values of 3.2 and 4.0, the polymer forms more easily and is more conductive than at higher values. ..... 43

Figure 4.3. Cyclic voltammogram of poly(methylene blue) formation on a platinum electrode. Sweep rate used was 100 mV/s for 25 cycles. Solution used for synthesis is shown in Table 4.3. Cycling limits are 1.0 $V_{SCE}$ and -0.5 $V_{SCE}$. ..... 45

Figure 4.4. Cyclic voltammogram of poly(methylene blue) formation on a polypyrrole coated stainless steel 304L electrode. Sweep rate used was 100 mV/s for 8 cycles. Solution used for synthesis is shown in Table 4.3. Cycling limits are 1.05 $V_{SCE}$ and -0.5 $V_{SCE}$. ..... 47

Figure 4.5. EIS equivalent circuit model used to determine charge transfer and other resistances of composite electrodes. $R_u$ is the ohmic resistance, $C_{dl}$ is the double layer capacitance with $R_{ct}$ being the curresponding resistance, $Z_W$ is the Warburg impedance for diffusion through the film and $R_L$ is the associated resistance, and $C_L$ is the capacitance representing the amount of reactive compound in the film. ..... 49

Figure 4.6. Comparison of complex plane impedance spectrum of bare polypyrrole on stainless steel and polypyrrole/poly(methylene blue) composite. Impedance was measured at 0 $V_{SCE}$ with a 10 mV amplitude between 100 kHz and 0.1 Hz. ..... 49

Figure 4.7. Change in the relative charge transfer resistance, as measured by EIS, of films with two different anions over time when stored in 50 mM pH 7 phosphate buffer. ..... 51

Figure 4.8. Confirmation of NADH oxidation on mediator-modified steel electrode. Oxidation peaks are from cyclic voltammetry scans at varying concentrations of NADH and at a 20 mV/s scan rate ..... 53

Figure 4.9. Open circuit voltage of *C. vulgaris* cathode microbial fuel cell across the transition from light to dark and dark to light cycles. A voltage drop of approximately 5 mV is seen when switching to the dark cycle ..... 56

Figure 4.10. Distribution of carbonate forms from dissolved $CO_2$ as a function of pH calculated by the Henderson–Hasselbalch equation with $pK_a$ values of 6.33 and 10.33 ..... 57

Figure 4.11. Response to a step change in voltage of biocathode/bioanode MFC with composite pPy/Poly(MB) anode and cathode electrodes. Voltage was stepped from open circuit (approximately 370 mV) to 270 mV. ..... 58

Figure 4.12. Transient view of polarization (voltage-current measurement) tests with bioanode and biocathode. Each voltage step is held for a duration determined to give 95% of the steady state current. ..... 59

Figure 4.13. Polarization curve with bio-cathode and chemical anode with different cathodic electrodes being compared. ..... 60

Figure 4.14. Polarization curve with bioanode (soluble mediator) with error bars. Data points are the average of three separate polarization curves on consecutive days and the bars are the range of the three measurements. ..... 62

Figure 4.15. Polarization and power curves for bioanode/biocathode microbial fuel cell with soluble mediator graphite anode and immobilized mediator steel cathode along with fit to basic model. Error bars show the relative standard deviation of current measurements..... 64

Figure 4.16. Polarization and power curves for microbial fuel cell with bioanode and biocathode each with an immobilized mediator steel electrode. Electrochemical resistance model fit lines shown. Error bars show the relative standard deviation of current measurements..... 65

Figure 4.17. Evolution of the open circuit voltage of a biocathode/bioanode microbial fuel cell after inoculation with a starter culture of *C. vulgaris* in the cathode and a dry culture of *S. cerevisiae* in the anode..... 66

Figure 4.18. Polarization curves showing the potentials of the anode and cathode separately. A reference electrode is placed in the anode and voltages are taken between each electrode and the reference. The cathode curve will include electrolyte resistance in this figure..... 68

Figure 4.19. Resistance of anode, cathode, and electrolyte with bio-anode and bio-cathode with immobilized mediator electrodes used for each. The negative slope of each line corresponds to the internal resistance of the given component at that current. ..... 69

Figure 4.20. Plot of voltage across the membrane and electrolyte in the MFC and a best fit line. Liquid junction (membrane) potential is shown at the zero current intercept and the slope represents the iR drop due to the ohmic resistance in the solution and the membrane. ..... 70

# NOMENCLATURE

## Symbols

| | | |
|---|---|---|
| a | Activation resistance parameter | $V/\log(mA/m^2)$ |
| A | Surface Area (of an electrode) | $cm^2$ |
| b | Ohmic resistance parameter | $\Omega\ m^2$ |
| C | Capacitance | F |
| E | Potential | V |
| $E^\circ$ | Standard potential | V |
| i | Current Density | $mA/m^2$ |
| I | Current | A |
| R | Resistance | Ω |
| $R_\Omega$ | Ohmic resistance | Ω |
| t | Time | s |
| V | Voltage | V |
| W | Warburg (diffusion) Impedance | Ω |
| Z | Impedance | Ω |
| $Z_{Re}$ | Real component of impedance | Ω |
| $Z_{Im}$ | Imaginary component of impedance | Ω |

## Greek Symbols

| | | |
|---|---|---|
| ϕ | Phase angle | ° |
| ω | Frequency | Hz, $s^{-1}$ |
| Π | Reaction quotient | varies |

# LIST OF ABBREVIATIONS

| | |
|---|---|
| AC | Alternating Current (used in EIS) |
| AQDS | anthroquinone-2,6-disulphonic disodium salt |
| CPE | Constant phase element (used in EIS modeling) |
| CV | Cyclic Voltammetry |
| DC | Direct Current (used in EIS) |
| EIS | Electrochemical Impedance Spectroscopy |
| MB | Methylene Blue |
| MFC | Microbial Fuel Cell |
| NADH | Nicotinamide adenine dinucleotide (reduced) |
| OCP/OCV | Open Circuit Potential/Voltage |
| PANI | Poly(aniline) |
| pPy | Poly(pyrrole) |
| SCC | Short Circuit Current |
| SCE | Saturated Calomel (reference) Electrode |

# 1. INTRODUCTION

Carbon dioxide emissions have become a prominent concern in recent years due to the rising level of atmospheric $CO_2$ and concerns about associated global warming. As a result, methods of carbon dioxide reduction have been of great interest. Photosynthetic organisms are an efficient means of reducing $CO_2$ using sunlight as the energy source. Microalgae such as those in the *Chlorella* genus have been the subject of research for carbon dioxide reduction, biofuel production, and waste treatment among others. More recently, photosynthetic organisms such as *Chlorella vulgaris* have been used as a unique biocathodes for microbial fuel cells (Cao, 2009; Powell, 2009).

Microbial fuel cells have been the subject of much investigation primarily for their potential use in treatment of organic wastewater, sources of power for remote devices, and electricity production tied to other bioproduct production. A recently proposed use of microbial fuel cells has been in the generation of electricity coupled to the reduction of $CO_2$ and production of bio oils associated with the growth of microalgae (Powell, 2011). Other biocathodes have been studied which use the reduction of oxygen or nitrate as the electron accepting reaction.

Anodes in microbial fuel cells typically use biofilms of bacteria grown on an electrode which allow direct electron transfer during anaerobic growth through various mechanisms. Alternatively, some of the earlier microbial fuel cell investigations used soluble electron mediators which interact with growing cells and transfer electrodes chemically to the electrode. In order to use microbes which produce valuable bioproducts such as ethanol, electron mediators are usually necessary, such as with the yeast *Saccharomyces cerevisiae*.

The need for some form of immobilized mediator arises when such microbial fuel cells are operated in continuous mode or on a large scale, at which time the cost and separation of mediators becomes a significant problem. In the past, methods of immobilizing electron mediators ranged from transition metal ions entrapped in carbon (Park, 2003) and conductive polymers doped with anionic redox compounds (Feng, 2010) to polymerized mediators on a noble metal surface for biosensors (Prieto-Simón, 2004).

A second problem arises when considering the scaling up of microbial fuel cells. The graphite electrodes which are typically used are physically weak and impractical for larger systems. The best performing alternatives are noble metals but these come with a prohibitively high cost. Stainless steel has been shown to work alone in sea floor microbial fuel cells that work because of the potential difference between the aerobic and anaerobic zones of the sea floor (Dumas, 2007). The performance of these systems is, however, quite low and their mechanism of action are not understood due to the mixed microbial culture.

In this project, a method of immobilizing an electron mediator on stainless steel (304L) has been developed by first applying a layer of polypyrrole which allows the electrode surface to remain electrically conductive at high potentials. This allows for the electropolymerization of redox dye mediators on the electrode surface. The resulting composite immobilized mediator has been tested individually in a photosynthetic biocathode using a pure culture of the microalgae *Clorella vulgaris* and in a completely biological microbial fuel cell with a *Saccharomyces cerevisiae* anode coupled to the aforementioned cathode. The performance of these systems has been compared to that reported by Powell et al. (2009; 2011) in which the same redox dye (methylene blue) and others were used as soluble electron mediators.

The following is an outline of the remaining chapters of this thesis. Chapter two, the background, provides the literature review and theory behind the experiments and research done. The literature review covers topics relating to the different types of microbial fuel cells, electrode types and electron transfer mechanisms, methods of analysis of microbial fuel cells and electrodes, and MFC modelling. Finally, a more detailed explanation of the project objectives is given.

Chapter three gives a detailed description of the experimental methods used for this work. First is a brief description of the equipment used, which is followed by the methods used for growing the microbes, preparing and analyzing electrodes, and doing the electrochemical analyses of the microbial fuel cell performance.

The fourth chapter is a discussion and presentation of the results of the experiments performed. Microbial fuel cells with photosynthetic microalgae biocathodes along with both chemical and biological anodes were compared with different electrode types. Several electrochemical techniques used to analyse the performance and a discussion of the effect of MFC operation on growth rate are included.

Chapter five contains the conclusions and recommendations derived from the research done for this thesis. It describes the successes and failures of the new electrode materials used in these novel microbial fuel cells and further work which could be done to improve upon them and to find more useful applications.

# 2. BACKGROUND

## 2.1 Microbial Fuel Cells

Microbial Fuel Cells (MFC) are an area of research which has seen a lot of interest in the past 10 years. They are seen as a promising technology for treatment of wastewater and renewable energy generation.

MFCs use the electrochemical potential created by oxidation or reduction of substrates to generate an electric current. Traditionally, only a microbial anode is used in which bacteria oxidise a substrate such as sugars, acetate, or organics contained in wastewater. In the absence of oxygen, instead of the electrons from the substrate oxidation going to oxygen, it is transferred to an electrode. For many species, this requires an electron mediator for this to take place as they cannot transfer electrons directly through their cell walls or membranes to an electrode. In these cases, a chemical cathode is used. These cathodes use either a precious metal catalyst to reduce oxygen at the cathode, much like chemical fuel cells or a more reversible chemical oxidizing agent dissolved in a cathode chamber such as potassium ferricyanide.

The anode and cathode are typically separated by cation exchange membranes or proton exchange membranes which allow positively charged ions to pass from the anode to the cathode maintaining pH and electroneutrality. Any ionically conductive separator can be used as long as it prevents mixing of the solutions but the ohmic resistance of the separator significantly affects the performance of the MFC.

Electron mediators are required for all but a few species of bacteria in order to facilitate transfer of electrons from microbe to electrode. These compounds, either by coming in contact with the microbes or diffusing through the cell walls, become reduced by the transfer of electrons from cellular electron transport molecules such as NADH. The mediator compounds are reversibly oxidized at the electrode surface, driving electrons to the cathode. Alternatively, some bacteria, when grown as biofilms, do not require mediators by one of three methods. First, they may secrete compounds into the extracellular part of the biofilm which act as mediators, they may contain cellular membrane proteins which allow electron conduction, or a few species contain conductive pili (Logan, 2009).

### 2.1.1 Types of Microbial Fuel Cells

Most microbial fuel cell research focuses on bacterial anodes with chemical cathodes (Qiao, 2007). Research involving soluble mediators has been extremely sparse in the past 5 years due to the use of bacteria which produce a current without exogenous mediators (Schröder , 2007; Logan, 2009). Some research has still been done with electrodes which promote electron transfer by immobilizing mediators or using nanotubes and other extremely high surface area materials (Qiao, 2007; Scott, 2007). Immobilized mediators have been shown to promote electron transfer in microbes which otherwise cannot produce an electric current on their own (Park, 2003).

A review of literature on bio-cathodes was done and the papers were mainly focused on aerobic and nitrate reducing cathodes. More information on biocathodes is presented in the following sections.

### 2.1.2 Substrates and Potentials

Substrates from simple sugars and acetate to natural and synthetic wastewater have been used in microbial fuel cells. The most common substrates used when high electrical performance is desired and aspects other than microbial growth are being studied are glucose and acetate. These are grown anaerobically in order to compel the cells to utilise an electrode (and subsequently the cathode) as the final electron acceptor instead of dissolved oxygen.

The maximum theoretical potential (voltage) created by a microbial fuel cell is dependent on the substrate, its concentration, and the type of cathode. The theoretical potential of the anode (with respect to a reference or to standard hydrogen scale) is calculated from the reference potentials of the components of the reaction or the Gibbs free energy of reaction:

$$E° = \frac{-\Delta G_r}{nF} \tag{2.1}$$

Combined with the Nernst equation and the reaction quotient (Π), this can be used to determine the theoretical potential at non-standard conditions:

$$E = \frac{-\Delta G_r}{nF} - \frac{RT}{nF} ln(\Pi) \tag{2.2}$$

The potentials of several half cell reactions relevant to microbial fuel cells are shown in Table 2.1 below. Potentials are reported at standard conditions as well as typical conditions in a microbial fuel cell (for example pH 7 instead of pH 1).

**Table 2.1. Half cell potentials of several substances used in microbial fuel cells calculated at standard conditions and at common microbial fuel cell conditions. [a](Logan, 2006).**

| Compound | Potential (vs. NHE) | |
|---|---|---|
| **Anode half reactions** | Standard Conditions | MFC (pH7, $C_{ox}=C_{red}$) |
| Acetate/$HCO_3^-$ [a] | -0.187 | -0.296 |
| $C_6H_{12}O_6/CO_2$ | -1.26 | - |
| **Cathode half reactions** | | |
| $O_2/H_2O$ [a] | 1.23 | 0.8 |
| $NO_3^-/NO$ | 0.96 | - |
| **Other** | | |
| Methylene Blue | 0.39 | -0.06 |
| Poly(methylene blue) | - | 0.11 |
| NADH/$NAD^+$ | -0.32 | - |
| $Fe(CN)_6^{3-/4-}$ | - | 0.45 |

### 2.1.3 Biocathodes

Aerobically grown bacteria produce a cathodic potential when grown on electrodes (You, 2009). Bacterial biofilms have been found to catalyze oxygen reduction on the cathodic electrodes of microbial fuel cells utilising electrons produced at the anode (Logan, 2009). Since the potential of the electrode is higher than the potential for oxygen reduction in cells, it becomes the preferential process and the cells will use the electrons from the anode as well as other carbon sources for energy.

Only one paper from other research groups has been published relating to cathodes based on photosynthetic reduction of carbon dioxide (Cao, 2009). In that work, a mixed culture of photosynthetic bacteria was used to reduce carbon dioxide at the cathode. They showed that

current can be generated through photosynthesis by a biofilm on the cathode without soluble mediators. It is unknown whether microalgae are capable of the same.

### 2.1.4 Photosynthetic Cathodes and Growth Rates

Powell et al. (2010) investigated a photosynthetic biocathode based using the microalgae *Chlorella vulgaris* to reduce carbon dioxide. The standard overall reaction for photosynthesis is the following:

$$6\ CO_2 + 12\ H^+ + 12\ e^- \rightarrow C_6H_{12}O_6\ (\text{biomass}) + 3\ O_2 \qquad (2.3)$$

where the $H^+$ and $e^-$ are normally supplied by water molecules. When an alternative electron donor is available, it may be utilized by the photosynthetic pathways. This relies on two criteria being met; first, the oxidation potential of the alternative electron donor must be lower than water so that it is the preferential reaction, and second, the alternative electron donor must be able to interact with the cells.

Powell et al. (2010) used methylene blue and 2-hydroxy-p-naphthoquinone (HNQ) (2011) as electron mediators. The standard reduction potential, E°, for water oxidation is 1.23 V compared to approximately 0.39 V (Ju, 1995) for methylene blue, indicating that it would be used preferentially.

These mediators were found to have an effect on growth rate. When used in a microbial fuel cell configuration, the growth rate of *C. vulgaris* was much lower in the presence of methylene blue. This was attributed to the reduction in the amount of light reaching the organisms (Powell, 2011). HNQ, on the other hand, was found to not block light and actually increased growth rate when used in a microbial fuel cell by a factor of 1.7 (Powell, 2011).

$CO_2$ concentration was found to have a notable effect on growth rate (Powell, 2010). Optimal growth rates were obtained when $CO_2$ mixed with air between 5 and 10% was added to the medium (either across the surface or bubbled). Mass transfer was not found to be limiting in any case because it was much faster than the uptake through microbial growth. The pH of the medium was found to have minimal effects on the growth, as some *Chlorella* species can utilise $CO_2$ in either its native dissolved form or as $HCO_3^-$. Many microalgae, however, can only utilise the native $CO_2$ form which favours lower pH media (Borowitzka, 1988).

One other use of photosynthetic reduction of $CO_2$ in a biocathode has been reported in which photosynthetic bacteria were used (Cao, 2009). In this case, no external electron mediator was used and organisms were grown as a biofilm on the electrode allowing either direct electron transfer or natural cellular mediators.

## 2.2 MFC Electrodes

Electrode materials and structures for microbial fuel cells have been the subject of a considerable amount of the MFC research in recent years. This review focuses primarily on anode materials because research on cathodes has almost exclusively been for chemical reduction primarily using platinum.

Metals which catalytically oxidize microbial metabolites have been used to generate additional power in the anode as well as to improve the electron transfer from the microbes themselves (Scott, 2007). Materials used include tungsten carbide (Rosenbaum, 2006) and platinum. These materials catalyze electrochemical oxidation of metabolites only so were not investigated further.

While most research to avoid the use of mediators has focused on a few species of bacteria with the unusual trait of being able to transfer electrons directly to a non-catalytic electrode, that approach precludes most organisms which produce a useful product. The polymer forms of several redox dyes have been studied for the similar application of enzyme-based biosensors (Silber, 1996) as solid surface electron mediators. Other surface-bound redox compounds have been used successfully to facilitate electron transfer in microbial fuel cells using bacteria (Feng, 2010).

Several studies have been done using polyaniline (PANI) and polypyrrole (pPy), electrically conductive polymers, in combination with various other substances to improve power generation in microbial fuel cells (Feng, 2010; Qiao, 2007). PANI and pPy are conductive polymers which help in electron transport and can partially eliminate the need for electron mediators. Their structure can also allow the transport of small molecules to active catalyst sites. Composites containing graphite, carbon nanotubes, carbon black (Scott, 2007), platinum black (Schröder, 2003), and anthraquinone-2,6-disulphonic disodium salt (AQDS) (Feng, 2010) have all been used to increase power generation in microbial fuel cells.

Rosenbaum et al. (2006) have investigated the use of tungsten carbide as a catalyst for the oxidation of microbial metabolites. Very high power densities have been achieved by using $H_2$ and formate producing bacteria. The formate and/or $H_2$ are then oxidized at the tungsten carbide anode surface. Similar power densities were achieved with tungsten carbide as with platinum anodes. Tungsten carbide has been studied as a catalyst with similar properties to platinum for the last 35 years. The oxidation of organic compounds (formate and lactate) was found to have a different mechanism for catalysis and was catalyzed by different tungsten compounds than $H_2$

was. They also found that significant corrosion of the tungsten carbide took place with ionic buffers near neutral pH.

Another method of improving performance of microbial fuel cells reported by Park et al. is to immobilize various electron mediators on the electrode surface (Park, 2003). Neutral red was found to have similar mediation potential immobilized on graphite as it does in solution. $Mn^{4+}$ and $Fe^{3+}$ were also found to significantly improve electron transport when immobilized on graphite electrodes. The highest power densities were achieved in a single chamber MFC with a $Mn^{4+}$ modified anode and $Fe^{3+}$ modified graphite cathode.

A form of graphite anode has been proposed which, unlike most carbon anodes, could be easily scaled up (Logan, 2007). Graphite fibres were bound in conductive titanium wires to form a brush (similar to a circular kitchen brush) to give a high surface area and open structure which prevents biofouling. Much higher power densities were achieved than traditional carbon paper electrodes. Ammonia treatment of carbon anodes was also proposed which places a negative charge on the anode to improve electron transfer. Graphite fibre brush anodes have been used in many subsequent microbial fuel cell studies.

Stainless steel electrodes were tested in a marine fuel cell in place of the traditional carbon electrodes (Dumas, 2007). Stainless steel was found to have lower performance than carbon but would be more easily scaled to larger geometries. Further study is required into the performance of stainless steel outside of ocean environments. Although not the focus of the paper, Manohar et al. (2009) showed that addition of stainless steel balls to a graphite anode decreased the cell resistance. This could be purely a result of increased surface area.

Morozan et al. (2007) found that the structure and composition of carbon anodes had a significant effect on the power generation potential. They found that higher power densities

were achieved when the anodes contained larger amounts of carbon nanotubes because of the nanotubes higher biocompatibility compared to other forms of carbon.

Heijne et al. (2008) studied graphite, Pt, and titanium anode electrodes. They found that the electrode surface resistance was lowest with Pt and highest with titanium. They also found that increasing the surface area of graphite simply by blasting it with $Al_2O_3$, the performance could be significantly increased beyond that of platinum.

Finally, Zhang et al. combined PTFE with graphite at the anode to achieve higher power densities than otherwise achieved (Zhang, 2007). When PTFE is combined with fine graphite particles, it forms a porous structure which creates a large surface area. The PTFE is also very hydrophobic which benefits electron transfer by attracting microbial cells to the surface. When PTFE content is too high, however, the electrical conductivity decreases and power output is reduced.

## 2.3 Polymerized Redox Dyes

A large number of enzymes involved in reducing organic matter depend on the coenzyme pair NADH/NAD+. Due to their oxidation and reduction properties and their reversible potentials near that of NADH and their non-toxic properties, redox dyes have been investigated as mediators for electron transfer between enzymes or microbes and an electrode (Chi, 1994). Many of these dyes have been shown to retain their redox activity upon electropolymerization on an electrode (Karyakin, 1999; Prieto-Simón, 2004). The films are also efficient catalysts for NADH oxidation similar to the monomers (Prieto-Simón, 2004) as shown by the large reduction in NADH oxidation overpotential when compared to an unmodified electrode. Poly(methylene

blue) has received much of the attention due to its favourable reversible potential and high stability as compared to other dyes (Karyakin, 1999).

Direct polymerization of the same mediator that is used in soluble form is promising and has been used for bio fuel cells and enzyme biosensors which rely on some of the same coenzymes as most used in microbial metabolism. Methylene blue retains its redox properties when polymerized on a surface (Karyakin, 1999) and has been used in the development of NADH dependent enzyme-based biosensors (Prieto-Simón, 2004). Methylene blue has only been polymerized on noble substrates such as precious metals and carbon materials before. For the above reasons, poly(methylene blue) has been investigated for use in enzyme biosensors. Poly(methylene blue) has been proposed to have the structures shown in Figure 2.1 below.

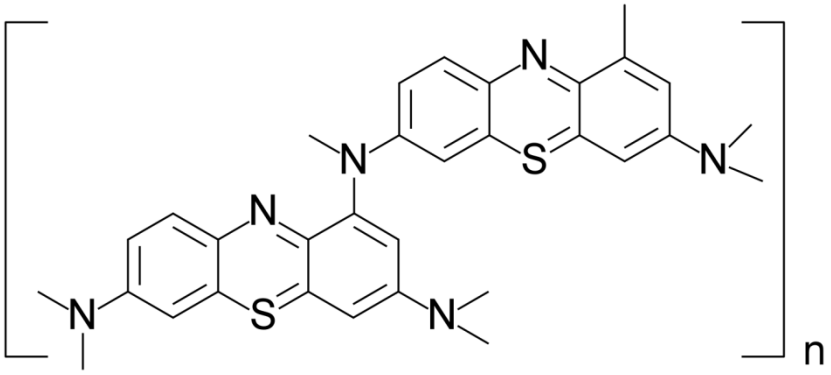


**Figure 2.1. Structure of polymerized methylene blue proposed by Karyakin (1999) with monomers joined at their nitrogen groups.**

## 2.4 Polypyrrole/salicylate

Previous investigations have been limited to the use of glassy carbon and noble metal substrates for the polymerization of redox dyes (Karyakin, 1999; Silber, 1996). At the potentials required for polymerization of methylene blue, an active metal would preferentially oxidize preventing film formation. Pyrrole, which can be converted to an electronically conductive

polymer (Vernitskaya, 1997), has been polymerized on stainless steel in solutions of nitrate or other anions with varying efficiencies (Schirmeisen, 1989).

Several studies have been done using conductive polymers in combination with various other substances to improve power generation in microbial fuel cells (Qiao, 2007; Feng, 2010). Other work into combining polypyrrole with possible electron mediators for biocompounds have mostly been with copolymers (Schuhmann, 1993; Wang, 2001) or polypyrrole with reversible redox ions as counter ions in the polypyrrole (Gros, 2004; Feng, 2010). Electrically conductive polymers have been shown to help with electron transport and can eliminate the need for electron mediators on their own in some cases.

When Feng et al. (2010) used polypyrrole for a microbial fuel cell electrode they used an anionic electron mediator, AQDS, with a potential just above that of NADH as the counter ion in polypyrrole as an electrode. The results showed a great improvement in power generation with a bacterial anode. Polypyrrole, as an electronically conductive polymer which can be relatively stable in water and can be deposited on non-noble metal substrates (Schirmeisen, 1989), appears to be one of the most practical materials for these applications.

Polypyrrole can be polymerized on non-noble metals through the use of certain anions as the supporting electrolyte. There have been reports of polypyrrole being used as a corrosion inhibitor on many different metals through two different mechanisms (Martins, 2004). The first, by ensuring a passive layer is always available by supplying charge to the surface, is not useful for microbial biocompatible electrodes. The second mechanism, which provides a complete barrier blocking oxidation of the metal, allows electron transport with a relatively low resistance between polymer and metal. A diagram showing the doped, oxidized (conductive) form of polypyrrole is shown in Figure 2.2.

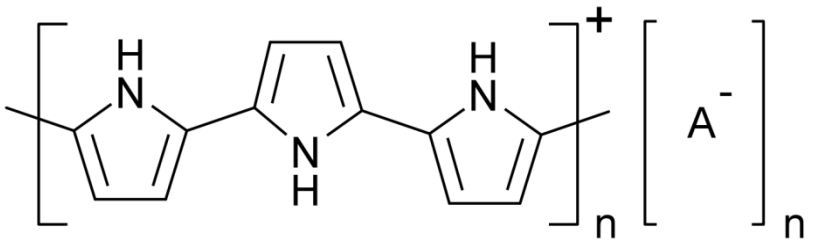


**Figure 2.2. Structure of oxidized (conductive) polypyrrole doped with an anion denoted by $A^-$. The polymer has a net charge of +1 for every three monomer units with partial positive charges on the nitrogen groups. Figure reproduced based on Vernitskaya et al. (1997).**

Anions used for polypyrrole formation on normal metals are usually such that they form an insoluble layer on the surface of the metal (the anion usually acts as a ligand) which is more conductive than the metal oxide which would otherwise be formed. This prevents further oxidation of the metal by blocking transport of ions away from the surface which in turn allows polymerization to be initiated. Ions used in for this purpose include malate, oxalate (Martins, 2004), and salicylate (Petitjean, 1999).

Polypyrrole is preferable to other conductive polymers for use on non-noble metals because of the relatively low potential required for its oxidative polymerization compared to others such as polythiophene and PANI.

## 2.5 Electrochemical Impedance Spectroscopy

Electrochemical Impedance Spectroscopy (EIS) is a popular method used to analyse the components of the overpotentials of an electrochemical cell. The cell is modelled as an equivalent electrical circuit with common electric circuit elements as well as some unique to EIS.

Small sinusoidal excitations in potential are applied to the system around the open circuit or reference potential. The frequency of these excitations is varied over many orders of magnitude

and the resulting current is examined to determine the impedance and phase angle of the system at different magnitudes of frequency.

A plot of the logarithm of the magnitude of the impedance and the phase angle against the logarithm of the frequency is called a Bodé plot. Alternatively, based on the magnitude and phase angle of the impedance, real and imaginary components of impedance can be calculated. In a Nyquist plot, the imaginary impedance is plotted on the y axis with the real component on the x axis. Both of these diagrams can be examined qualitatively to determine the processes limiting the potential of the system. Usually, however, a circuit is used to model the system and the values of the circuit elements are chosen which give the same impedance spectra as the electrochemical system (Orazem, 2008).

The simplest circuit commonly used to model an electrode/electrolyte system is a Randles cell, which contains a resistor, due to the resistance of solution and the electrode, and a parallel combination of a capacitor and resistor which are due to the charge transfer resistance from the electrolyte to the electrode and the associated double layer capacitance. The charge transfer resistance varies with current density (often modeled using the Butler-Volmer equation) so EIS experiments are often done at the open circuit potential or other potentials which are being used for further experiments.

When the electrode in an electrochemical system is non-homogenous (either the surface properties are not uniform or the geometry is such that the surface concentrations vary across the electrode), the double layer capacitance is usually replaced with a constant phase element (CPE). A CPE is similar to a capacitor but the dependence of the admittance on frequency is not linear. While the admittance of a capacitor is represented by $j\omega C$, a CPE's admittance is represented by $(j\omega)^n Q$. Q is analogous to capacitance, C, but cannot be viewed as the true capacitance of the

system as can be seen by the difference in units (C is in units of S·s and Q is in units of $S \cdot s^n$). It has been suggested that the true capacitance be calculated by: $C = Q\omega_{\max}^{n}$ where $\omega_{\max}$ is the frequency at which the imaginary component of the impedance is at a maximum.

The circuit models above neglect one of the three typically described overpotentials in electrochemical cells, the mass transfer or concentration overpotential. When there is a concentration gradient near the electrode due to the limited rate of diffusion of reactants, the concentrations at the electrode surface are different than those in the bulk electrolyte. According to the Nernst equation,

$$E = E^{0'} + \frac{RT}{nF}\ln\frac{C_O}{C_R} \tag{2.4}$$

The potential varies with the concentration of reactants at the electrode surface, not the bulk concentration. The difference between the potential based on the bulk electrolyte concentrations and those actually observed is called the concentration overpotential.

The simplest circuit element used to describe diffusion effects is the Warburg impedance. A Warburg impedance is at a constant phase angle of $45^o$ regardless of frequency with a magnitude of $\sqrt{2}\sigma/\omega^{1/2}$ where $\sigma$ is the Warburg constant. Physically, a Warburg impedance represents semi-infinite diffusion in the electrolyte. The Warburg coefficient depends on the concentrations, diffusion coefficients, and stoichiometry of the redox reaction according to equation 2.5 (Bard, 2000).

$$\sigma = \frac{RT}{n^2F^2A\sqrt{2}}\left(\frac{1}{D_O^{1/2}C_O^{\infty}} + \frac{1}{D_R^{1/2}C_R^{\infty}}\right) \tag{2.5}$$

Where n is the number of electrons transferred per reaction, F is Faraday's constant, A is the area of the electrode, $D_O$ and $D_R$ are the diffusion coefficients of the reactants and $C_O^\infty$ and $C_R^\infty$ are their bulk concentrations.

When diffusion is occurring through a limited diffusion layer outside of which the bulk electrolyte is at constant concentrations, the impedance element used is 'porous bounded Warburg', or 'O' element. At high frequencies it is the same as the Warburg element, but at lower frequencies, the imaginary component of impedance begins to decrease and eventually goes to zero. The impedance of the 'O' element is given by equation 2.6 (Orazem 2008).

$$Z = \left( \frac{1}{Y_0 \sqrt{j\omega}} \right) \tanh\left(B\sqrt{j\omega}\right) \qquad (2.6)$$

Where $Y_0$ is related to the Warburg coefficient by $\sigma = \frac{1}{\sqrt{2}Y_0}$ and B is related to the diffusion coefficient and diffusion layer thickness by $B = \frac{\delta}{\sqrt{D}}$. This element is of particular interest in rotating disk electrode (RDE) experiments and for electrode coatings, where the diffusion layer thickness is finite.

## 2.6 Microbial Fuel Cell Analysis and Modelling

Simple models for microbial fuel cells consist of quantifying internal resistances by various methods. More advanced models have attempted to predict the physical processes in the microbial fuel cell including electrochemical kinetics, mass transfer, and microbial growth in one or more dimensions.

### 2.6.1 Components of microbial fuel cell resistances

The ohmic resistance consists of the resistance to electron conduction through the circuit as well as ion conduction through electrolyte and membrane in an electrochemical cell or fuel cell. Usually the ionic portion of the resistance constitutes the majority of the overall ohmic resistance. Phosphate or carbonate buffers are typically used to decrease the resistance of the electrolyte (Fan, 2007). The resistance in the electrolyte is inversely proportional to the concentration of the buffer solution but varies between different ions. In two chamber microbial fuel cells, the membrane is the primary component of the ohmic resistance.

The anode polarization or activation resistance in a microbial fuel cell is the resistance to the reduction involving microbial fuel cells or mediators at the electrode surface. Most microbial fuel cells which use an oxygen reduction cathode, the cathode activation resistance is much higher than that of the anode (Fan, 2008). The activation resistance for microbial fuel cells is usually linear with current density at typical operating conditions. When biofilms are present, the activation resistance has been found to be proportional to the electrode surface area (Fan, 2008).

The microbial metabolism resistance is the internal resistance due to the limited rate at which substrate can be oxidized. In many lower power density microbial fuel cells, this is the primary limitation. If the substrate or biomass concentration is limiting, the current will not increase significantly with decreased voltage. The resistance will be proportional to anode volume as well as biomass and substrate concentration.

The mass transfer resistance is a common limitation in chemical fuel cells (O'Hayre, 2006) but is less commonly encountered in microbial fuel cells. When the electrode reaction is

relatively fast and current densities are high, transport of charge from the electrolyte to the electrode can cause a concentration gradient. When modelling such systems that are stirred it is often treated as a bulk solution with constant concentration and a thin diffusion-only layer near the electrode surface (Picioreanu, 2007; Marcus, 2007). This diffusion layer with a concentration gradient can also arise in systems in which a biofilm is formed on the surface which prevents convective mixing in that region.

A simple non-dimensional model for the flux to an electrode and corresponding current current density are given in equations 2.7 and 2.8 (O'Hayre, 2006).

$$J = D \frac{C_\infty - C_0}{\delta} \tag{2.7}$$

$$j = nFD\frac{C_\infty - C_0}{\delta} \tag{2.8}$$

Where D is the diffusion coefficient, C is the concentration, and $\delta$ is the diffusion layer.

### 2.6.2 Electrochemical Techniques

Several electrochemical methods have been used to study microbial fuel cells (MFC). Slow potential sweeps are used to generate polarization curves. Cyclic voltammetry is commonly used to determine oxidation potentials for microbial metabolism in biofilm-based cells. Electrochemical impedance spectroscopy (EIS) has been used recently to study the components of the internal resistances in a cell. Other less common techniques have been attempted with varying levels of success.

Most researchers use potential sweeps to generate voltage-current (cell polarization curves) (Schröder, 2003) and power-current curves and to determine the maximum power output of the

cell (Logan, 2006). Maximum power output has been shown to occur when $R_{int} = R_{ext}$ (Manohar, 2008).

Ohmic losses in MFCs have been successfully determined using the current interruption technique and by other techniques such as impedance spectroscopy (Manohar, 2008; Qiao, 2007). These techniques can be used to qualitatively determine whether ohmic losses, polarization resistance, or mass transport losses dominate based on the shape of the curves.

Cyclic voltammetry (CV) has also been used extensively in the analysis of MFCs (Manohar, 2009; Schröder, 2003; Logan, 2006). CV is generally used to determine the electrochemical activity of microbial cultures in the anolyte solution. It has been used successfully to determine the mechanism of direct electron transfer from microorganisms in a biofilm to an electrode (Fricke, 2006).

The use of electrochemical impedance spectroscopy (EIS) in the analysis of microbial fuel cells has only become common in the last three years (Manohar, 2008; Manohar, 2009; Qiao, 2007). By doing EIS measurements and fitting a simple circuit (one-time constant model, OTCM), the solution resistance, polarization resistance, and electrode capacitance can be determined as well as the individual polarization resistances of the two half cells (Manohar, 2008). Using Ohm's law and measurements for the half cells, the membrane resistance can also be determined for two chamber MFCs (Manohar, 2009). By performing EIS measurements at several potentials, more information can be determined about the overpotentials and the dependence of internal resistance on current. Model parameters have shown a good fit to the EIS data but no EIS studies have been found for cases in which mass transfer effects were studied likely due to the natural fluctuations present over the low frequencies required.

Differential pulse voltammetry has been proposed as an alternative to CV in studying oxidative potentials of different systems (Marsili, 2008). For systems which take a long time to reach their pseudo-steady state potential, this method can reduce the amount of time for the experiments. No reported uses of differential pulse voltammetry for MFCs were found in literature.

A unique and powerful method to determine various components of the internal resistance was done by Fan et al. (2008). They assumed each component of the resistance was proportional to some experimental parameter (ie. Surface area). By varying the parameter and measuring the polarization curve, one can determine the specific contribution of that resistance. They use this method to find anode, cathode, membrane and electrolyte resistances.

### 2.6.3 Polarization and Power Curves

Polarization or voltage-current curves have become the standard method of presenting microbial fuel cell performance (Logan, 2006) as is the case with chemical fuel cells. Not only does this show the maximum current and open circuit voltage of the cell, but it shows characteristics of the voltage-current behaviour which give an indication of the types of internal resistances which are predominant.

There is considerable variation in the techniques and methods of reporting these curves. First, some authors do a short potential sweep which does not allow the system to reach steady state at any one voltage or current (often leading to over reporting of performance), while others use a fixed voltage or resistance until steady state is reached. Additionally, current is usually reported as a density normalized to chamber volume or electrode area. Electrode areas, however

are not consistent as some reports use the geometric surface area of porous structured carbon materials while others report based on true surface area.

### 2.6.4 Modelling

Although microbial fuel cells have been studied extensively in the lab by many researchers, very few attempts have been made to develop mathematical models of these systems. The simplest electrochemical models used to fit the performance of microbial fuel cells are based on the surface reaction kinetics, electrolyte (ohmic) resistance, and mass transfer effects. It is the same technique used for chemical fuel cells (O'Hayre, 2006) and is useful mainly for comparisons and not for obtaining absolute values of any parameters. Such models also only work for predicting and modelling steady state conditions.

These simple models depict the potential as a function of current density (i), equilibrium potential, activation resistance, electrolyte resistance, and concentration or mass transfer resistance. The thermodynamic potential is represented by the symbol $E^0$. The activation overpotential is represented by the term ($a + b \ln i$), the electrolyte overpotential by $R_\Omega i$, and the mass transfer overpotential by $c \ln i_L/(i_L\text{-}i)$. Overall, the equation depicting the performance of the microbial fuel cell is shown in equation 2.9 (for the case of a reversible cathode; O'Hayre, 2006).

$$E = E° - (a + b\, lni) - R_\Omega i - c \ln\left(\frac{i_L}{i_L - i}\right) \qquad (2.9)$$

Where a, b, and c are constants determined experimentally, $R_\Omega$ is the overall ohmic resistance of the electrolyte, electrodes, and membrane, and $i_L$ is the mass transfer limited current density. $E^\circ$ and a can be combined when fitting to experimental data. In the case of a non-

reversible cathode, the activation terms can be combined into one so that a and b represent the terms for the combined anode and cathode.

The first transient physical model, which was for a system with an added soluble mediator compound and freely suspended cells, was published in 1995 by Zhang and Halme (1995). It was a transient model which considered only the mass balances and reactions but not mass transfer effects. It assumed the entire chamber was well mixed and that the cathode was at a constant potential.

Other, more complex, models specific to microbial fuel cells was published more than ten years later by Picioreanu et al. (2007) and others (Marcus, 2007). Their models were focused on modelling the biofilm growth and current generation in microbial fuel cells with a diffusion layer near the electrode and in the biofilm. The first of these models was solved numerically in 1, 2, and 3 dimensions for the anode side only. Picioreanu et al. (2008) later combined their MFC model with a previously published anaerobic digestion model for the oxidation of glucose by bacteria.

Zeng et al. (2010) presented a model of a microbial fuel cell which follows the general modelling approach used for hydrogen PEM fuel cells. It is an electrochemical model with the incorporation of Monod kinetics for substrate oxidation and an oxygen reduction cathode. The model doesn't consider mass transfer effects near the electrode. The researchers did extensive measurements on a lab-scale MFC and fit parameters to the model so that it accurately predicted the performance of the cell.

Ganguli et al. (2008) found some important parameters and reaction mechanisms for a yeast-catalyzed microbial fuel cell with methylene blue mediator. They developed a model of the RDE system with a two step reaction, mediator reduction and yeast reduction/substrate oxidation. The

model with mediator reduction being the limiting step was found to fit the experimental data and rate constants for the reaction were determined. The mechanism they found for the yeast/mediator system is shown in Equations 2.10 and 2.11 (Ganguli, 2008).

$$M + Y^R \xrightarrow{k_M} M^R + Y \tag{2.10}$$

$$Y + S^R \xrightarrow{k_E} Y^R + S \tag{2.11}$$

Where M is the mediator, Y is the yeast cells, S is the substrate, superscripts of R represent the reduced form and a lack of superscript represents the oxidized form. The mediator/electrode (surface) reaction was found to be reversible in this case and therefore not rate limiting.

## 2.7 Detailed Objectives

The objectives of this research project were originally to evaluate the use of alternative electrode materials, primarily involving base metals such as steel, in the novel type of microbial fuel cell investigated previously by the research group of Dr. Hill (Powell, 2009; Powell, 2011). When the possibility of creating electrodes which preclude the use of soluble electron mediators arose, the focus of the research shifted to these materials in combination with different electrode supports. The goal for the microbial fuel cell experiments was to compare and evaluate the performance of these systems to the traditional microbial fuel cell setup involving soluble mediators and graphite electrodes, both in the novel, photosynthetic biocathode, as well as a coupled microbial fuel cell with a traditional anode utilising yeast. A schematic diagram of the interaction of microbes, mediators, electrodes and electrolytes is shown in Figure 2.3.

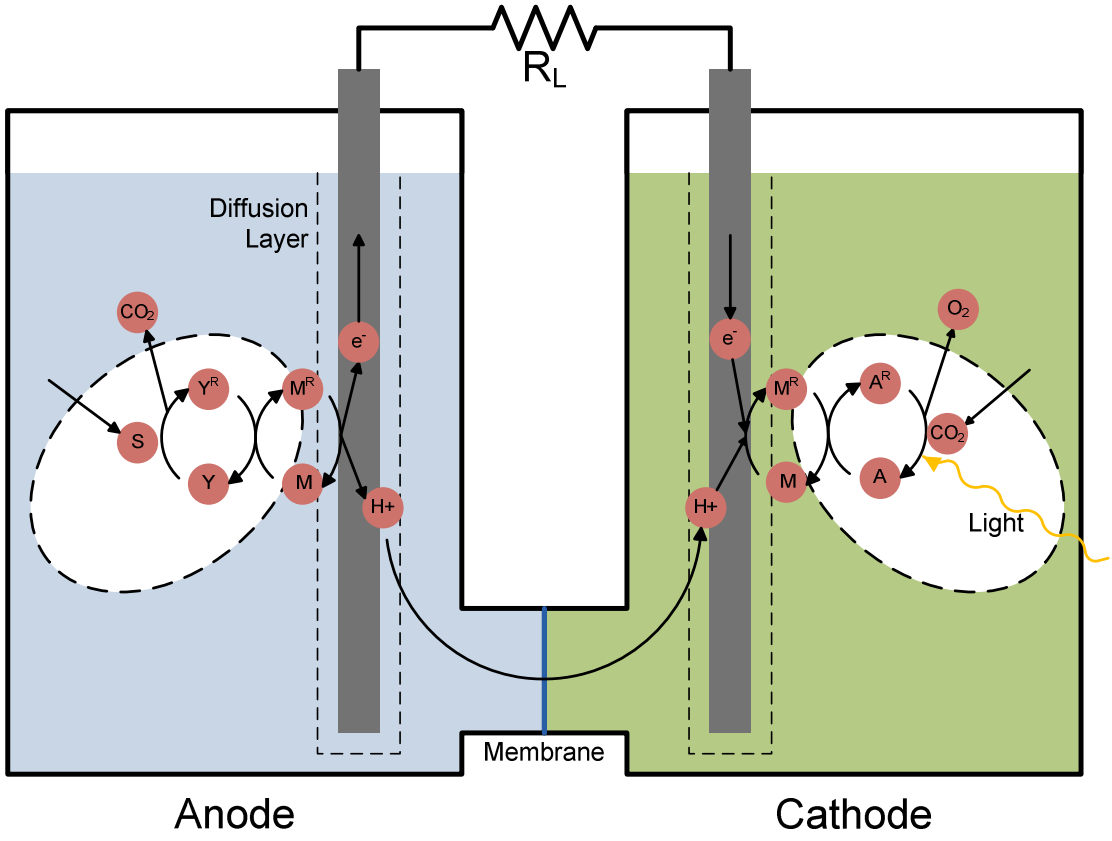


**Figure 2.3. Diagram of a microbial fuel cell with a yeast bioanode and algae biocathode. A represents algae cells, Y represents yeast cells with superscripts 'R' representing the reduced state for those cells. S is the yeast substrate (glucose) and M is the mediator compound, either attached to the electrode or in solution depending on the experiment.**

# 3. EXPERIMENTAL

## 3.1 Equipment

For all electrochemical experiments and polymerizations, potentiostats from Gamry Instruments were used. For electrochemical impedance measurements, a Gamry G-750 potentiostat was used which is capable of measuring at frequencies up to 100 kHz. The software used to control the EIS experiments was EIS300™ Electrochemical Impedance Spectroscopy Software. For all other electrochemical experiments, a Gamry Reference 600 potentiostat was used along with the PHE200™ Physical Electrochemistry Software. These programs are operated from within the Gamry Framework 5.6 Software.

Analysis of electrochemical results (EIS, CV, etc.) were analysed using the Gamry Echem Analyst software which is able to fit equivalent circuit models to EIS data and find CV peaks and other important parameters as well as exporting data to Microsoft Excel for plotting.

Stirring was performed with Hanna instruments stir plates.

## 3.2 Methylene Blue Polymerization

Methylene blue was first polymerized on non-oxidizing substrates: platinum, gold, and glassy carbon. This is an electrochemical oxidation process wherein the methylene blue in solution is polymerized at the positively charged surface of the working electrode. The standard method for performing this reaction is by cycling the potential of the electrode from below the reversible redox potential up to a potential high enough for the oxidative polymerization to take

place. With each successive sweep, more polymer is deposited. Aside from creating more adherent films than potentiostatic methods, this method also allows visualization of the polymer growth by observing the increase in the size of the reversible polymer oxidation peak with each potential sweep.

The setup is a typical three electrode cell with the working electrode, platinum mesh counter electrode, and saturated calomel reference electrode placed in the solution and connected to a Gamry Reference 600 potentiostat which performs voltage control and current measurements. A 25 mL three electrode cell was used with the glassy carbon working electrode of 0.0707 $cm^2$.

Electrodes were polished with diamond paste and progressively finer alumina using an electrode polishing kit to give a mirror surface.

Initially, solutions of methylene blue, sodium borate (as a buffer), potassium nitrate, and potassium hydroxide (to adjust pH) are prepared to the desired pH and species concentrations. Methylene blue concentrations of 0.5 to 4 mmol/L were used and pH values between 7 and 11 were examined. Nitrate and borate concentrations of 0.1 mol/L and 0.025 mol/L were used, respectively for all experiments. Due to variations in literature parameters, peak potentials of between 0.8 and 1.1 $V_{SCE}$ were tested. Cyclic voltammograms were run for 12 to 15 cycles depending on when the monomer oxidation peak had disappeared and the polymer peak stopped increasing.

For all further experiments after optimization, values of 1 mmol/L methylene blue, 9.5 pH, and a 1.05 $V_{SCE}$ peak potential were used. The cyclic voltammetry was performed at a rate of 100 mV/s with a minimum potential of -0.5 $V_{SCE}$.

## 3.3 Stainless steel electrode preparation

Stainless steel 304L rods were obtained from Steelmet (Saskatoon, Canada). These rods were cut to the lengths needed and had a diameter of 6.35 mm (1/4 in). For the experimental preparation and optimization of the composite films, steel rods were coated in epoxy and only the end was polished. Polishing was performed by sanding with 600 grit sandpaper followed by alumina to give a mirror finish. This exposed end gave a consistent surface area of 0.32 $cm^2$. After sanding, the end was thoroughly rinsed with acetone to remove any metal particles and water limiting oxidation of the steel surface.

## 3.4 Polypyrrole synthesis

Polypyrrole synthesis, when needed as a surface coating, is performed by electropolymerization at constant current (galvanostatically) or constant potential (potentiostatically). When polymerized on non-noble metal substrates, a doping ion which is a ligand must be used to limit oxidation of the metal while the polymer is being formed. The metal-ligand forms a very thin insoluble layer which blocks metal ions from dissolving but still allows oxidation of pyrrole at the surface.

Doping ions for polypyrrole used with stainless steel include oxalate, salicylate, and nitrate, all of which were tested experimentally. Three electrode cells were used. For the optimization experiments with 0.32 $cm^2$ electrodes, a 25 mL cell was used with saturated calomel reference and platinum counter electrodes. Current was controlled and potential was measured with a Gamry Reference 600 in galvanostat mode. For all polypyrrole syntheses, the cell was purged with nitrogen to prevent oxidation of the pyrrole in solution by oxygen in the air.

The solution for polypyrrole synthesis consisted of 0.25 mol/L pyrrole in water with 0.1 mol/L doping ion and just enough phosphoric acid to reduce the pH to the desired level (which was varied between 3 and 6). The galvanostatic method was used for all experiments for a duration which gave the lowest final potential (approximately corresponding to the most conductive film). A current density of 6 $mA/cm^2$ was found to be optimum in this respect and was used for all further experiments. The polymerization time used was 180 seconds as this was the average point when the minimum potential was achieved.

## 3.5 Composite electrodes and microbial fuel cell electrode preparation

Deposition of poly(methylene blue) on polypyrrole was performed in the same way as on bare electrodes as described in section 3.2. The resulting cyclic voltammogram characteristics were more difficult to discern but the current peaks could be seen increasing and desired resulting properties were achieved. Due to the potential for methylene blue monomers adsorbing to the polypyrrole in addition to the polymer form, the electrodes were soaked in water for at least 1 hour before any further use.

In order to use the composite electrodes for microbial fuel cell experiments, a higher surface area was needed. In this case, the stainless steel rods were polished as described earlier, but not coated in epoxy. The rods were immersed in a long, narrow three electrode cell along with the saturated calomel reference and counter electrode. In this case, graphite rods were used as counter electrodes because of their higher surface area and similar geometry to the steel.

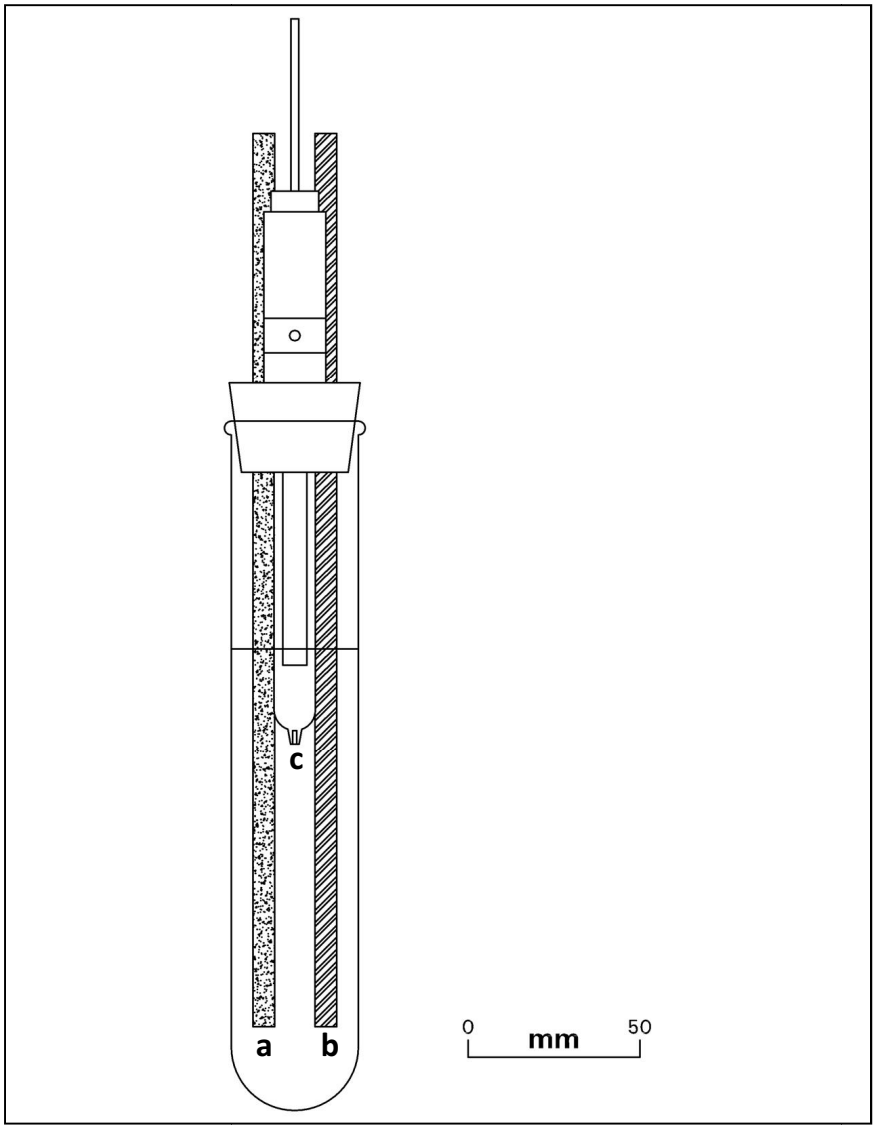


**Figure 3.1. Microbial fuel cell electrode preparation cell. A graphite rod (a) is used as the counter electrode, stainless steel (b) as the working electrode onto which the polymer layers are deposited, and a saturated calomel (c) reference.**

A diagram of the setup used for the microbial fuel cell electrode preparation is shown in Figure 3.1. This cell was used for both the polypyrrole deposition as well as for poly(methylene blue). The steel rods were immersed 6 cm into solution giving an approximate total surface area of 11 $cm^2$. All current values were adjusted based on previously determined current densities.

## 3.6 EIS analysis of electrode coatings

Coatings were analysed for stability when stored in electrolyte solutions using electrochemical impedance spectroscopy. Between readings the electrodes were immersed in a phosphate buffer solution with a pH of 7.0 and a phosphate concentration of 50 mmol/L. For EIS measurements, the electrodes were placed in a 25 mL three electrode cell with SCE reference and platinum counter electrodes in the same solution used for storage.

A Gamry potentiostat was used for the EIS measurements in potentiostatic EIS mode with a DC voltage of 0 V and an AC voltage magnitude of 10 mV. A frequency range of 100 kHz to 0.1 Hz was used for all EIS experiments.

The model described earlier (section Modelling2.6.4) was implemented in the Gamry Echem analyst software so that the data could be fit to the model. The Simplex method was used for data fitting with initial estimates of parameter values obtained by observing the Nyquist plot of the impedance data. Values of $R_{CT}$ and capacitance were recorded for comparisons and calculations.

## 3.7 NADH catalysis measurement

In order to confirm that poly(methylene blue) adhered to the electrode and is still active, the current obtained from CVs in different concentrations of NADH was measured. Solutions of NADH in water were prepared at concentrations of 0, 1, 3, 5, and 7 mmol/L. At each of these concentrations, the electrode was immersed in the solution in a 25 mL three electrode cell with SCE reference and platinum counter electrodes. Cyclic voltammetry was performed between +0.4 $V_{SCE}$ and -0.6 $V_{SCE}$. The peak oxidation currents were determined with the Gamry Echem software for comparison.

## 3.8 Algae culture for microbial fuel cell biocathodes

*Chlorella vulgaris* was obtained from Carolina Biological Supply and was stored in a refrigerator until used. Bold's Basic medium (James, 1978), a standard used for growing green microalgae, was used as the growth medium for starter cultures as well as for microbial fuel cell experiments. The contents of the medium are shown in Table 3.1.

**Table 3.1. Bold's Basic medium nutrients and minerals.**

| Nutrients | Conc. (mg/L) |
|---|---|
| $NH_4Cl$ | 75 |
| $MgSO_4 \cdot 7H_2O$ | 50 |
| $K_2HPO_4$ | 100 |
| $KH_2PO_4$ | 150 |
| $CaCl_2$ | 25 |
| NaCl | 25 |
| Na·EDTA | 50 |
| **Trace Elements** | |
| $FeSO_4 \cdot 7H_2O$ | 4.98 |
| $H_3BO_3$ | 11.42 |
| $ZnSO_4$ | 8.82 |
| $MoO_3$ | 0.71 |
| $Co(NO_3)_2 \cdot 6H_2O$ | 0.49 |
| $MnCl_2$ | 1.44 |
| $CuSO_4 \cdot 5H_2O$ | 1.57 |

The media was prepared in one litre batches and sterilized before being used.

The starter cultures were grown in flasks at room temperature under fluorescent plant growth lights providing approximately 4000 lx of light intensity. Timers were used to control the lights to be on for 16 hours out of every 24. Electrochemical experiments were done during the light phase unless otherwise specified.

Cultures were stirred only enough to keep the cells from precipitating with magnetic stirrers. For the starter cultures, no $CO_2$ supplementation was provided and no other gasses were blown into the flasks.

Starter cultures were incubated for at least two weeks before being used to inoculate the microbial fuel cell biocathode. By this time, the cultures were a uniform, bright green colour.

The biocathode was first operated alone with a chemical anode. Two one litre bottles were joined by a 5 $cm^2$ Nafion-112 proton exchange membrane which had been previously activated with 4 M sulphuric acid and stored in water. Lids were placed on the bottles to prevent outside air from mixing into them. Electrodes were inserted through holes in the lids and held in place by rubber stoppers, which also provided an airtight seal. Each bottle was cleaned in an ultrasonic bath and rinsed with ethanol for sterilization before use. 500 mL of the Bold's medium was added to the cathode bottle and inoculated with approximately 50 mL of starter culture.

A bubbler was used in the cathode which supplied 8% $CO_2$ mixed with air at a flow rate of 200 mL/min. Pre-calibrated gas flow meters were used to mix the industrial grade $CO_2$ with air. The bottles were placed on stir plates with and stirred continuously.

For the biocathode experiments, the anode was filled with 500 mL of 20 mmol/L potassium ferrocyanide. Due to the gradual shift in potential of this reducing agent, a saturated calomel reference electrode was used in the anode to measure the potential against while the ferrocyanide still acts as an electron donor.

## 3.9 Yeast Growth and Microbial Fuel Cell Bioanode

*Saccharomyces cerevisiae* was used as a bioanode in a microbial fuel cell with glucose used as the substrate. The medium used was an expensive (chemical) medium used by Wall et al. (1992), the contents of which are shown in Table 3.2.

These citrate concentrations give a pH of approximately 4.1. The substrate was sterilized before use by boiling for 1.5 hours. Final cultures were observed under a microscope to ensure bacterial contamination had not occurred.

Inoculation of the bioanode was done directly with the dried yeast. Any electrodes being used were inserted at the time of inoculation and the anode chamber remained closed and airtight during growth to ensure anaerobic conditions. The magnetic stirrer was adjusted to a speed which prevented excessive settling of yeast cells. However, due to the design of the cell, settling was unavoidable in the bridging section between anode and cathode.

**Table 3.2. Yeast substrate used for bioanode studies.**

| Minerals | Conc. (g/L) |
|---|---|
| $NH_4Cl$ | 2.50 |
| $Na_2HPO_4$ | 2.91 |
| $KH_2PO_4$ | 3.00 |
| $MgSO_4$ | 0.25 |
| $CaCl_2$ | 0.08 |
| **Buffer** | |
| Citric acid | 5.30 |
| Trisodium citrate | 2.50 |
| **Nutrients** | |
| Yeast extract | 3.00 |
| **Substrate** | |
| Glucose | 20 to 50 |

Measurements of performance including open circuit potential, voltage-current behaviour, and response times were carried out in the stationary phase of growth, which is achieved after approximately 24 hours with the glucose concentrations used here. This was the point at which the potential reached a maximum and allowed more reproducible voltage and current generation behaviour.

The physical setup of the microbial fuel cell described in this and the previous section is shown in Figure 3.2.

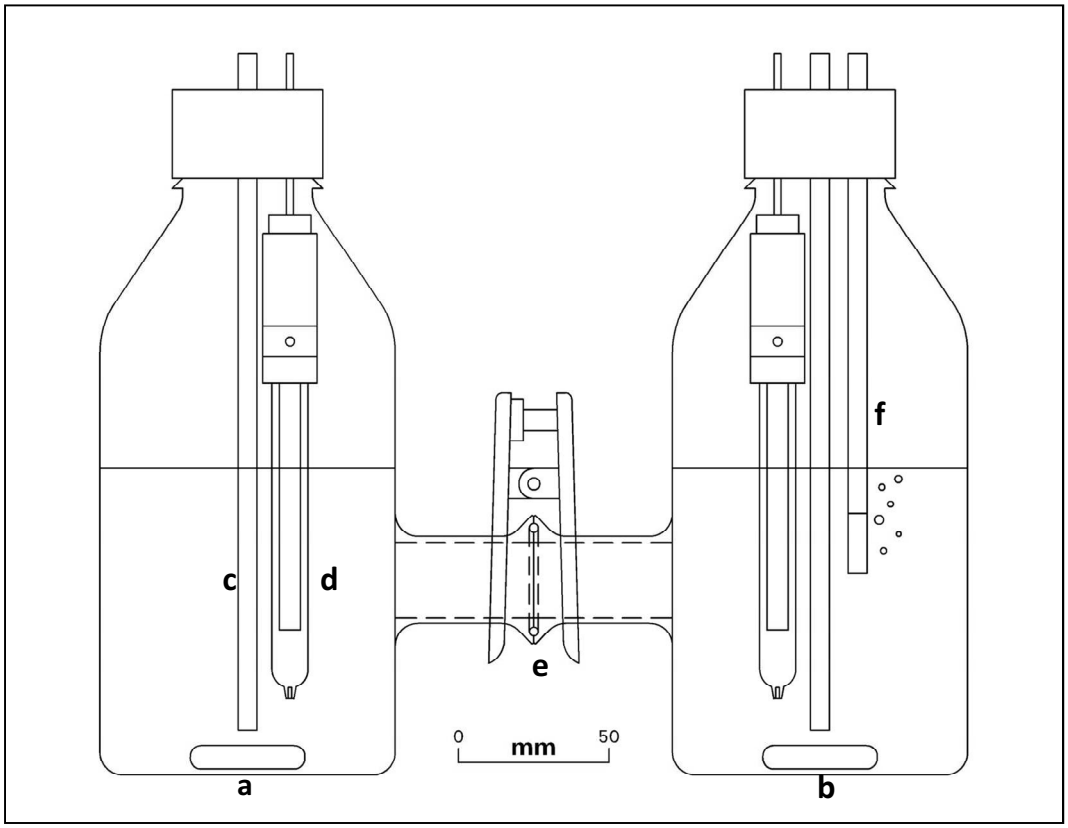


**Figure 3.2. Microbial fuel cell apparatus showing the anode (a), cathode (b), working electrode (c), reference electrode (d), Nafion-112 membrane (e), and $CO_2$ bubbler (f).**

## 3.10 Microbial Fuel Cell Analysis Procedures

Microbial fuel cell setups were analysed by measuring their open circuit potentials, transient response times, steady state polarization curves, and values obtained from them. Components of

the internal resistance were analysed electrochemically as shown below. Additionally, some basic cell culture characteristics were measured such as substrate pH and cell concentration.

### 3.10.1 Cell Growth and Biomass Concentraitons

Cell growth rates were not measured directly, although biomass concentration was found to stabilize two to three days after algae culture inoculation. Biomass concentrations were measured before microbial fuel cell experiments and after they were completed. For the concentrations measurements before MFC operation, 50 mL of solution was removed and centrifuged for 5 minutes. The centrifuged cells were left to dry at room temperature for 48 hours and weighed again and the biomass concentration calculated. The measurements after completion of experiments were done by the same method but the entire solution was weighed and centrifuged due to the significant weight of the biofilm.

### 3.10.2 Open Circuit Voltages

Open circuit voltages were measured with a potentiostat using the open circuit voltage experiment. The working electrode leads were connected to the cathode electrode and the counter and reference leads to the anode electrode. The experiments were set to have a duration of 3600 s and the final, stable reading was taken as the OCV.

### 3.10.3 Measuring and Plotting Polarization Curves

Polarization curves were plotted with steady state current and voltages. Some authors do a short potential sweep which does not allow the current to reach steady state which artificially increases the current values. Instead, multiple potential steps were done and held for times determined to give 95% of the steady state current (section 4.2.4). These final current values are

divided by the exposed (geometric) electrode surface area to give current densities and reported in $mA/m^2$.

### 3.10.4 Measuring Internal Resistances

There have been many different methods used to measure microbial fuel cell internal resistances. In this research, a new method was used to differentiate the anode and cathode internal resistances from the ohmic resistance due to the electrolyte and membrane. Reference electrodes were placed in each chamber near their respective working electrodes. Voltage current curves are recorded as before but in this case, the voltage between the reference electrodes and the anode are recorded as well. This allows determination of the potential across the electrolyte and membrane (between the two reference electrodes), potential of the anode (with respect to a reference and disregarding the electrolyte resistance), and the same for the cathode by simple subtraction.

# 4. RESULTS AND DISCUSSION

## 4.1 Formation and Evaluation of Metal-based Immobilized Mediator Electrodes

While most research to avoid mediators have focused on a few species of bacteria with the unusual trait of being able to transfer electrons directly to a non-catalytic electrode, those organisms mean that the only product is electricity and no useful products can be produced (without genetic manipulation). The polymer forms of several redox dyes have been studied for the similar application of enzyme-based biosensors as solid surface electron mediators (Silber, 1996). Other surface-bound redox compounds have been used successfully to facilitate electron transfer in microbial fuel cells using bacteria (Feng, 2010).

Polypyrrole was selected as a conductive polymer layer because it is relatively stable in aqueous solutions, is stable in the potential ranges required for mediator polymerization and microbial fuel cell operation, and can be electropolymerized directly on an electrode surface.

Methylene blue has been chosen as a polymerizable mediator because it is one of the most stable of the polymerized redox dyes (Karyakin, 1999) and retains similar redox potentials after polymerization. It was also used in soluble form in the microbial fuel cell which this work takes inspiration from (Powell, 2011) and has favourable redox potential compared to NADH. Neutral red was also investigated but not found to have favourable redox potentials once polymerized. The redox peaks on the CV were 0.5 V lower than those for methylene blue.

Stainless steels, nickel, and carbon steel were investigated as non-noble metal electrode substrates on which to form layers of polypyrrole then poly(methylene blue). Several counter

ions and preparation methods were attempted in order to get stable, adherent immobilized mediator films. Ultimately stainless steel 304L was found to be the only suitable metal of the ones investigated and was used for microbial fuel cell experiments. A diagram showing the charge transfer in such electrode films is shown in Figure 4.1.

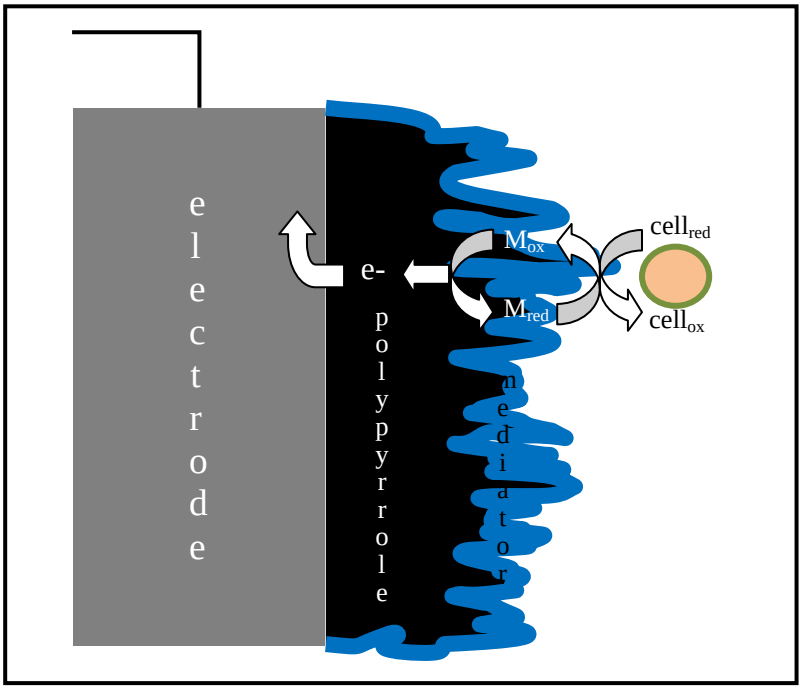


**Figure 4.1. Expected electron transfer mechanism between microbial cells and composite immobilized mediator electrode with polypyrrole and poly(methylene blue).**

### 4.1.1 Conductive Polypyrrole Used to Block Oxidation of Metal Surfaces

Polymerized mediators cannot be deposited directly on to base metals or alloys because the metal oxidizes at lower potentials than the oxidative polymerization. In case of iron, this causes a large current due to continuous dissolution of iron into solution. With stainless steel (304L), metal is initially oxidized but a passive film of metal oxides soon prevents current from flowing also preventing oxidation of mediator at the metal surface. Such a passive film would also prevent electron transfer from the mediator to the electrode itself.

Polypyrrole is one of the most stable conductive polymers and can be formed by electropolymerization. It is in the conductive form in the oxidized (black) state when subjected to potentials above -0.5$V_{SCE}$ so long as it does not become over oxidized. Below -0.5V, the doping anions leave the polymer and it becomes reduced and insulating. Overoxidation, somewhere above 1.2 $V_{SCE}$ causes degradation of the films.

Polypyrrole was selected as an interface between the stainless steel electrode and the polymerized mediator because it is stable in all of the conditions used. The synthesis parameters for polypyrrole affect its stability, structure, and conductivity.

### 4.1.2 Formation of Conductive Polypyrrole on Base Metal Alloys

In order to use a polypyrrole coated electrode in a microbial fuel cell, a uniform, conductive coating with good stability needed to be obtained. On stainless steels, only certain doping ions can be used in order to prevent oxidation of the steel itself from being the dominant process during electropolymerization.

Three anions which have been shown to work as the doping ion for polypyrrole formation on steels were tested: nitrate (in the potassium salt form), oxalate (oxalic acid), and salicylate (sodium salt). Polypyrrole is typically formed at low pH values, between 2 and 6.

For all tests, pyrrole was polymerized galvanostatically (constant current) on the electrodes. The first indication of the level of success is the shape of the resulting voltage-time plot. If the potentially quickly peaks then continues to decrease, the film is conductive and the increased surface area of the film lowers the overpotential required for polymerization. If the potential begins to increase, it means either that the film is not as conductive or not adhering to the metal

surface. Alternatively, if the potential does not peak in the first few seconds, it is likely that the metal is oxidizing in preference to pyrrole polymerization.

**Table 4.1. Success of different anions as the counter ion during pyrrole polymerization.**

| Metal | Anion | | |
|---|---|---|---|
| | Nitrate | Oxalate | Salicylate |
| Nickel | x | x | x |
| S.S. 304L | √ | x | √ |
| Carbon Steel | x | x | x* |

*visible polypyrrole layer formed but was not uniform and not conductive

The preceding table (4.1) shows the different combinations of metal electrode and anion used and whether or not they were successful, based on the formation of a uniform, visible film, and the chronopotentiometric plot (voltage-time plot with a constant applied current). Nickel proved unsuccessful in all attempts. Although some visible polypyrrole could be applied on carbon steel, it was not uniform and spots of corrosion could be seen between areas of the polymer. Polymerization was successful on 304L stainless with two anions, nitrate and salicylate, which were investigated further.

Figure 4.2 shows some of the voltage-time plots for successful and unsuccessful polymerizations. Based on these plots, the optimal polymerization time was determined to be the point at which the potential reached a minimum before beginning to increase. In the case of salicylate and stainless steel 304L, this was between 180 and 200 seconds.

Various pH values for the synthesis solution were tested to determine which gave the most consistent, uniform polypyrrole coatings as shown in Figure 4.2. pH values of 3.2, 4, 5, and 6

were initially used. Using 6 did not give any visible polypyrrole and 4 gave the most uniform coating. Ultimately, a pH of 4.5 was found to give the best results in terms of decreasing voltage on the choronopotentiometry experiment and a uniform coating.

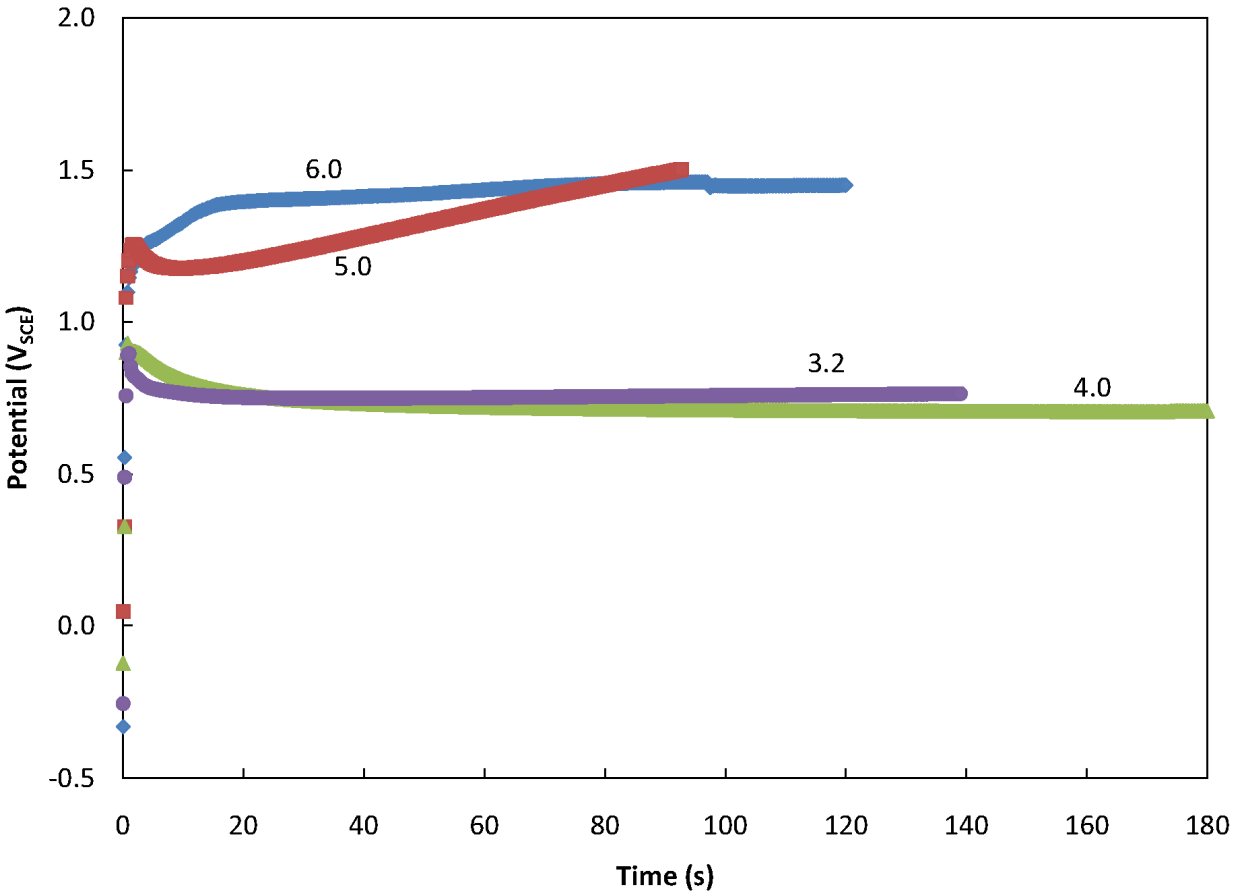


**Figure 4.2. Chronopotentiometry plots for deposition of polypyrrole on stainless steel 304L from solutions of different pH (shown as labels). At values of 3.2 and 4.0, the polymer forms more easily and is more conductive than at higher values.**

Impedance spectroscopy measurements were done for each of the successful polypyrrole electrodes, as well as for the poly(methylene blue)/polypyrrole electrodes produced later. It was found that consistent charge transfer resistances of 100 to 150 ohms were achieved for bare polypyrrole when the chronopotentiometry plot indicated a successful polymerization.

The current density used for polymerization was 6 $mA/m^2$. Polymerization could not be initiated to produce a continuous film with lower concentrations or lower current densities due to preferential oxidation of the steel. However, when the current density and pyrrole concentrations were high enough, the initial film formed quickly enough to inhibit further oxidation of the steel. After the initiation of the film, the potential reached a steady value of approximately 0.8 V which depends strongly on the current density and pyrrole concentration. The solution used for electropolymerization is shown in Table 4.2.

**Table 4.2. Pyrrole solution used for polymerization on stainless steel.**

| Compound | Concentration (mol/L) |
|---|---|
| Phosphate | ~$1 \times 10^{-3}$ |
| Salicylate | 0.1 |
| Pyrrole | 0.25 |
| pH | 4.5 |

Polymerization was attempted on carbon steel as well as nickel with nitrate, salicylate, and oxalate anions. Tests were done potentiostatically in order to determine whether the initiation of complete coverage films could be achieved. At all potentials attempted, little or no polymer was visible. In the case of carbon steel, current would increase indicating the oxidation of the metal was faster than polymerization. In the case of nickel, current would go to zero which indicates that a passive film is formed before polymerization can be initiated. In all cases, the metals were sanded and polished with alumina and ethanol before experiments began.

### 4.1.3 Formation of Poly(methylene blue) on Polypyrrole Coated Steel

Initially, methylene blue polymerization was performed on non-reactive substrates (glassy carbon, gold, and platinum) by the cyclic voltammetry technique as reported in literature (shown in Figure 4.3). The irreversible oxidation takes place near 1 $V_{SCE}$ to create the polymer form of methylene blue. The reversible oxidation and reduction peaks of the monomer are preserved in the polymer centered around -0.28 $V_{SCE}$ shifting positive to -0.15 $V_{SCE}$ for the polymer. Several parameters, pH, counter ion, concentration, switching potential, were varied to optimize the polymerization with a glassy carbon working electrode. The optimum was found to be a solution of pH 9.5 at 1 mM methylene blue with nitrate supporting electrolyte and a maximum potential of 1.05 $V_{SCE}$. Optimum films were considered to be those with a narrow polymer oxidation peak which continues to grow with further voltage sweeps.

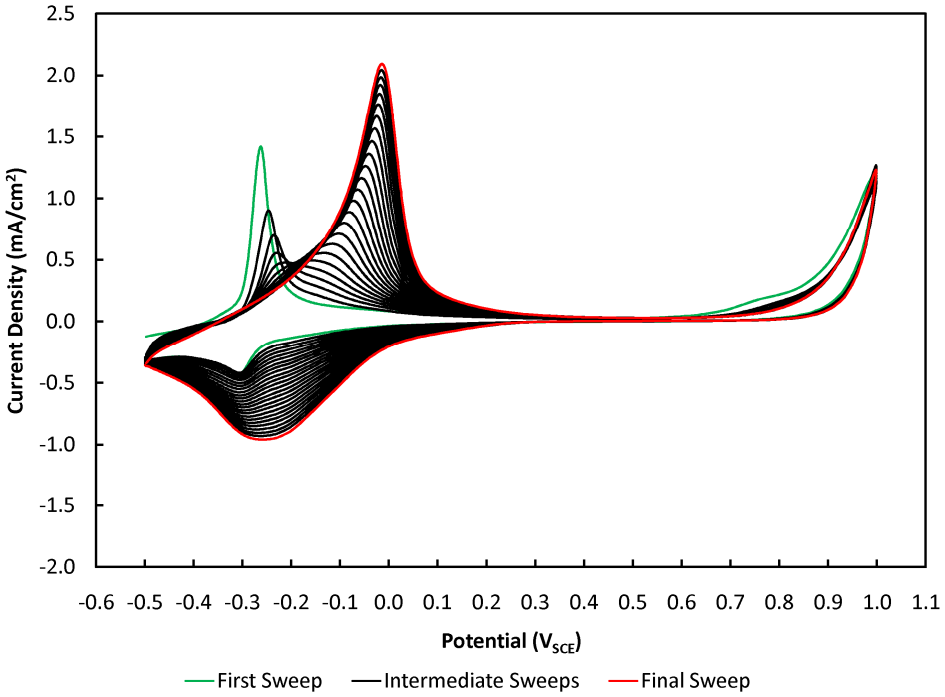


**Figure 4.3. Cyclic voltammogram of poly(methylene blue) formation on a platinum electrode. Sweep rate used was 100 mV/s for 25 cycles. Solution used for synthesis is shown in Table 4.3. Cycling limits are 1.0 $V_{SCE}$ and -0.5 $V_{SCE}$.**

At several of the solution compositions, no polymerization was possible. Only at high pH values and with nitrate in the solution was a polymer layer observed after the voltage sweeps.

Stability when stored in water was moderate with a half deactivation time, based on CV oxidation peak, of a few days (less than the 2 weeks reported previously (Karyakin, 1999). Methylene blue polymerized on graphite rods (which have a somewhat porous structure) shows a much longer stability time, with little decrease in charge transfer resistance (measured by impedance spectroscopy) after 2 weeks.

The optimal methylene blue polymerization solution composition is shown in Table 4.3.

**Table 4.3. Methylene blue synthesis solution composition.**

| Compound | Concentration (mol/L) |
|---|---|
| Potassium ($K^+$) | 0.175 |
| Nitrate ($NO_3^-$) | 0.1 |
| Borate ($BO_3^{3-}$) | $25 \times 10^{-3}$ |
| Methylene blue | $1 \times 10^{-3}$ |
| pH | 9.5 |

The optimum values for peak potential, methylene blue concentration, and pH found from the non-reactive electrode optimization were used for the composite films with polypyrrole. It was found that on polypyrrole-based electrodes, the optimum number of cycles is between 8 and 12, after which the current peaks on the cyclic voltammogram no longer increase.

A cyclic voltammogram of the polymerization of methylene blue on a polypyrrole coated electrode is shown in Figure 4.4. The peaks that form are much broader than on the smooth non-reactive electrode (Karyakin, 1999) due to the microstructure of the polypyrrole and its own

redox activity. The high background current also obscures the peak corresponding to monomer oxidation beyond the first potential sweep. It was also observed that if the lower switching potential was too low (below -0.5 $V_{SCE}$) the poly(methylene blue) peak would not appear with successive potential sweeps. This is due to conversion of polypyrrole to its reduced non-doped state which has been found to be non-conductive (Vernitskaya, 1997).

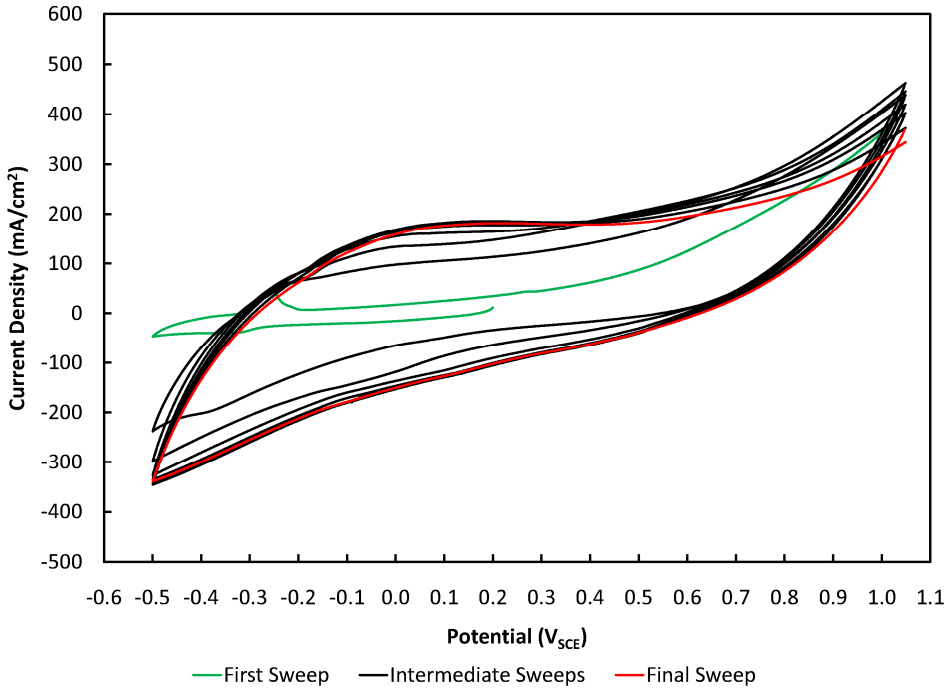


**Figure 4.4. Cyclic voltammogram of poly(methylene blue) formation on a polypyrrole coated stainless steel 304L electrode. Sweep rate used was 100 mV/s for 8 cycles. Solution used for synthesis is shown in Table 4.3. Cycling limits are 1.05 $V_{SCE}$ and -0.5 $V_{SCE}$.**

As with methylene blue on non-reactive electrodes, the evidence for actual polymerization as opposed to simple adsorption is shown by two aspects of the cyclic voltammogram. The first is the formation of a peak at a more positive potential than that of the monomer, see Figure 4.4. Adsorbed methylene blue shows an oxidation peak at the same potential as that of the monomer (Ju, 1995). The second is the oxidation peak at the switching potential of 1.05 V with no

corresponding reduction peak. In addition, the methylene blue would not likely remain on the surface for the amount of time found in the stability tests due to diffusion.

Attempts were made to polymerize methylene blue directly on the surface of non-noble metals such as stainless steel, nickel, and titanium. However, in all cases, the oxidation of the metal at potentials near 1 V was rapid and prevented any polymerization of methylene blue. The formation of polypyrrole takes place at a low enough potential and with a high enough rate to form a boundary which blocks the oxidation and dissolution of metal ions.

### 4.1.4 Measurement of Film Impedance and its use in Evaluating Film Performance

Ferloni et al. (1996) proposed equivalent circuit models and fitting procedures for the impedance of the electrically conductive polymers polypyrrole and polythiophene. The model has been used for the composite polymer since the processes are largely the same except for a much smaller charge transfer resistance. The equivalent circuit used is shown in Figure 4.5. The first two sections are typical for any realistic electrochemical cell with Ru being the ohmic resistance and the constant phase element with the value of $C_{dl}$ and parallel resistance representing the charge transfer at the electrode boundary. The Warburg impedance in parallel with a resistance represents diffusion of charged species through the polymer film. The final capacitance represents the overall redox charge capacity of the film.

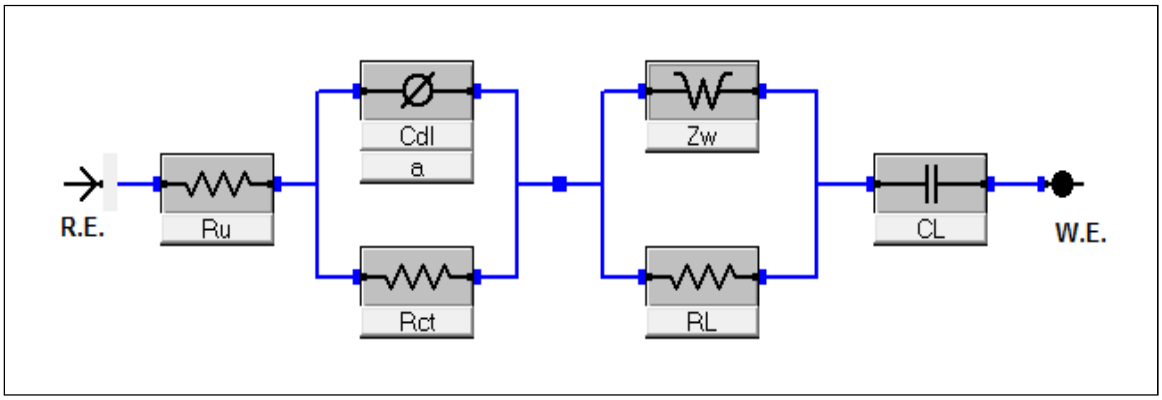


**Figure 4.5. EIS equivalent circuit model used to determine charge transfer and other resistances of composite electrodes. $R_u$ is the ohmic resistance, $C_{dl}$ is the double layer capacitance with $R_{ct}$ being the corresponding resistance, $Z_W$ is the Warburg impedance for diffusion through the film and $R_L$ is the associated resistance, and $C_L$ is the capacitance representing the amount of reactive compound in the film.**

The parameter compared for all films is the charge transfer resistance, which corresponds approximately to the width of the high frequency arc in the complex plane plot (Figure 4.6).

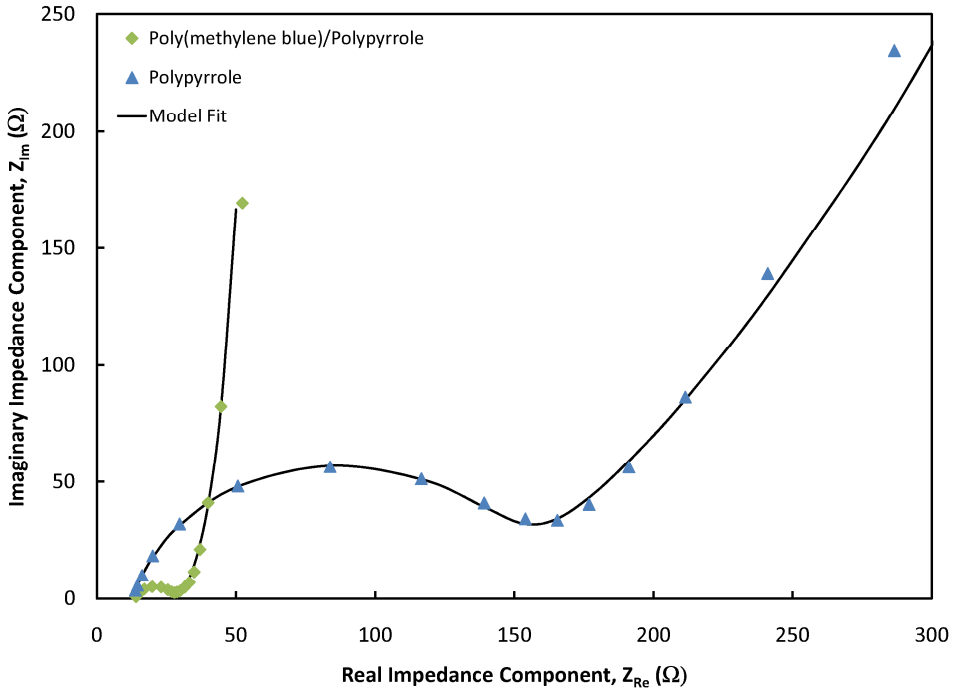


**Figure 4.6. Comparison of complex plane impedance spectrum of bare polypyrrole on stainless steel and polypyrrole/poly(methylene blue) composite. Impedance was measured at 0 $V_{SCE}$ with a 10 mV amplitude between 100 kHz and 0.1 Hz.**

Figure 4.6 shows the impedance of the composite film compared to a bare polypyrrole film using potentiostatic EIS at 0 $V_{SCE}$. The impedance depends strongly on the DC voltage and thus 0 V was used for all experiments since it is near the reversible potential of methylene blue.

### 4.1.5 Degradation of Films in Aqueous Solutions

In order to evaluate the stability of the films in aqueous solution, electrodes were aged in phosphate solutions and impedance spectra were recorded periodically. The charge transfer resistance was measured by fitting the data to the circuit model described previously. Charge transfer resistance was measured over time and the time for its doubling is reported. The impedance is also compared to bare polypyrrole as a reference.

Figure 4.7 shows the increase in charge transfer resistance with time for the composite polypyrrole/methylene blue films with two different polypyrrole counter ions. The doubling times for the charge transfer resistances were 16 hours for the polypyrrole with nitrate and 67 hours for that with salicylate anion. Two samples using nitrate are shown to demonstrate the repeatability of the test and of the material durability.

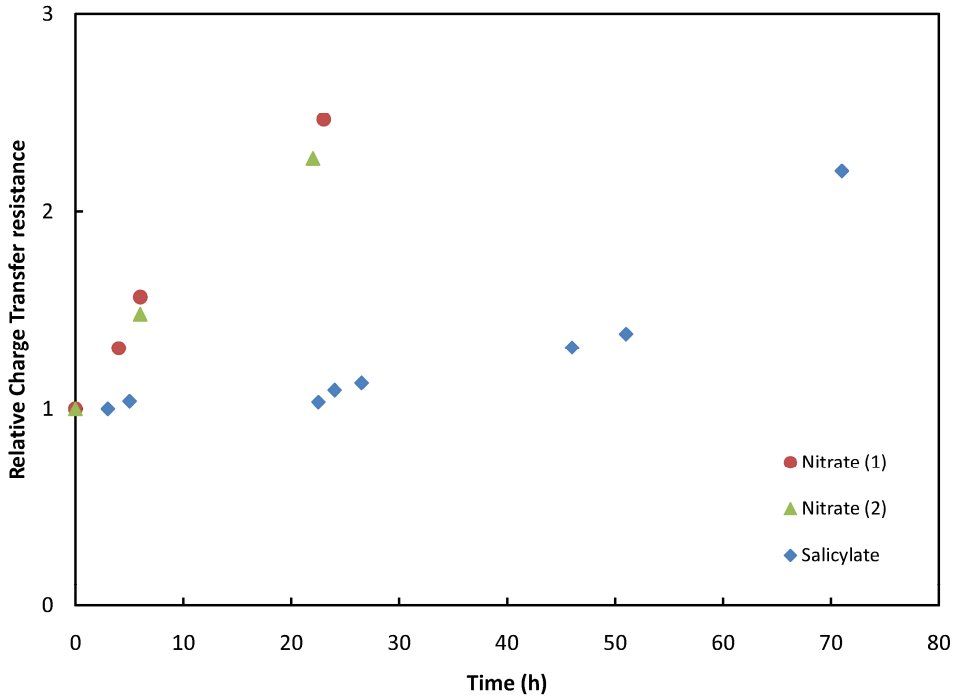


**Figure 4.7. Change in the relative charge transfer resistance, as measured by EIS, of films with two different anions over time when stored in 50 mM pH 7 phosphate buffer.**

### 4.1.6 Comparison of the Use of Different Doping Ions in Polypyrrole

Various factors determine the stability of polypyrrole in aqueous solution including the choice of anion (Wang, 2001). Two factors have been identified which can potentially influence the loss of activity due to ion loss. Ions are lost when the positively charged groups on the polymer are reduced so an ion that causes slower reduction of the polymer is more stable. Additionally, larger anions are less mobile which acts as a barrier to further reduction of the polymer while maintaining electro-neutrality.

Polypyrrole formation on stainless steel has been shown to be more efficient in nitrate than other solutions (Schirmeisen, 1989) so initially nitrate was used as the dopant. The stability in nitrate was very limited, as shown by the charge transfer resistance doubling time of only 16 hours seen in Figure 4.7.

Salicylate was chosen because it is a larger anion which is only moderately soluble in neutral and acidic solutions and is relatively stable. As well, polypyrrole has been grown previously on steel in the presence of salicylate (Petitjean, 1999). The charge transfer resistance starts out at approximately the same value with salicylate and nitrate anions within experimental variability. The resistance quickly increases with time for nitrate but much more slowly for salicylate-based polypyrrole. The doubling time for the charge transfer resistance was 67 hours for salicylate, a factor of 4 increase over that with nitrate. The relative charge transfer resistance, compared to the initial charge transfer resistance, is shown in Figure 4.7 for nitrate and salicylate.

### 4.1.7 NADH Oxidation as a Method of Confirming Bioelectrochemical Activity

Interest in poly(methylene blue) has been largely due to its catalysis of NADH oxidation for use in biosensors or other devices relying on NADH dependent enzymes. In order to determine whether the poly(methylene blue) films on polypyrrole coated stainless steel also promote NADH oxidation, cyclic voltammograms were performed between +0.4 $V_{SCE}$ and -0.6 $V_{SCE}$. The resulting peak heights are shown in Figure 4.8.

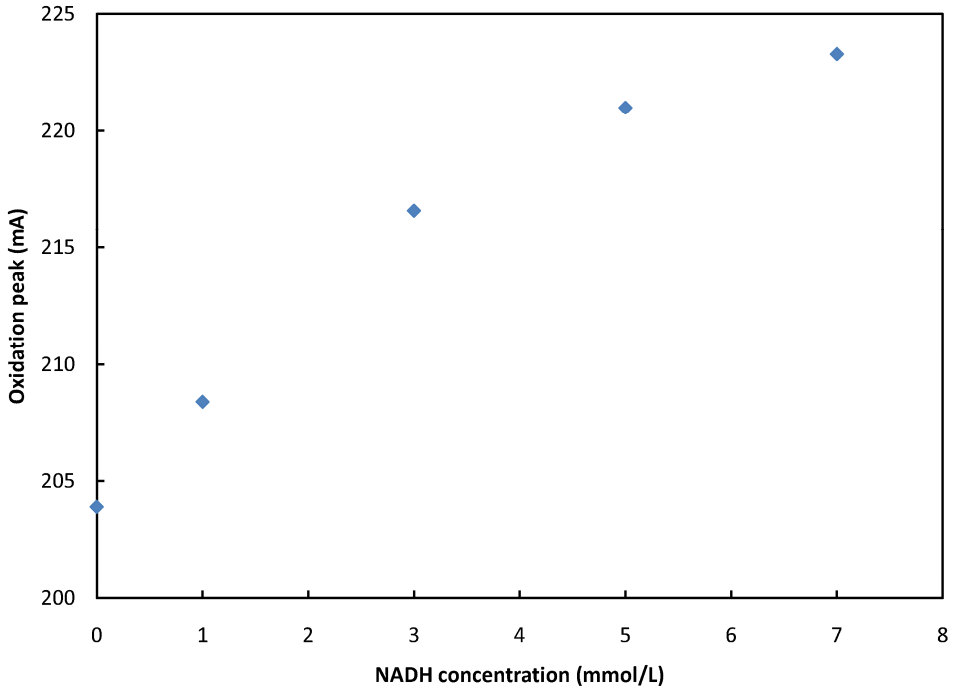


**Figure 4.8. Confirmation of NADH oxidation on mediator-modified steel electrode. Oxidation peaks are from cyclic voltammetry scans at varying concentrations of NADH and at a 20 mV/s scan rate.**

Even with no NADH present, the background peak current on the CV was over 200 mA. The background current was due to oxidation of the methylene blue itself as well as capacitive and redox effects of the polypyrrole which were also seen on the poly(methylene blue) formation CV (Figure 4.4). The oxidation peak height was found to increase slightly with addition of NADH. The increase appeared to be linear up to approximately 3 mM NADH after which the slope decreased as seen in Figure 4.8.

The high background current and slow response times with the electrode films being studied would make them less suitable for biosensor applications than thin films without a background current. However, in applications such as bio fuel cells in which a high steady state current is desired, these films may be more applicable.

## 4.2 Photosynthetic Biocathodes with Immobilized Mediator Electrodes

The second phase of the research, after the development and analysis of electrode coatings, involved testing the electrode materials previously developed in a microbial fuel cell environment. One of the primary goals of this research was to use $CO_2$ reducing cathodes utilizing *Chlorella vulgaris* with improved electrodes. The central methods used to evaluate performance were to measure the open circuit potential and the cell polarization curves. The former gives an indication of the efficiency of the microbes in converting their substrate to energy. The polarization curves, plots of the steady state current versus potential across the cell between the open circuit and short circuit, give an indication of overall performance potential and internal resistance. The effect of microbial fuel cell operation on the growth of *Chlorella vulgaris* has been examined previously by Powell (2010).

### 4.2.1 Microbial Fuel Cell Operation

The biocathode microbial fuel cell was operated with a chemical anode consisting of 20 mmol/L potassium ferrocyanide. Due to the unstable potential of the anode solution, potentials were measured with respect to a saturated calomel reference electrode in order to give consistent, comparable results.

The fluorescent plant growth lights were situated 30 cm above the cell cultures giving a measured light intensity of 4000 lx at the level of the glass surface. The same types of lights were found to have a spectrum with peaks at wavelengths of 450 nm and 670 nm (Powell, 2009). The maximum growth rate for *Chlorella sp.* was found to occur at intensities between 4000 and 20000 lx (Borowitzka, 1988). This compares to a maximum intensity from sunlight of approximately 100000 lx.

When the cathode was inoculated with the starter algae culture, the solution was initially a uniform transparent pale green colour. As growth continued in the microbial fuel cell, the solution became a darker green. A biofilm could be seen forming on the surface of the electrode. Biofilm formation in microbial fuel cells is typically due to the enhanced growth caused by the interaction of the microbes with the electrode, which was observed for *C. vulgaris* by Powell et al. (2011). Open circuit potentials were also seen to be higher after the formation of these biofilms.

When examined under a microscope, the matrix binding the cells together, typically consisting of carbohydrates, was visible. Large areas of the cells were relatively immobile due to the gel-like consistency of the biofilm. The extracellular matrix was a slightly green colour, likely from dead cells.

### 4.2.2 Biocathode Open Circuit Potentials

The open circuit potentials were measured across the biocathode microbial fuel cell between the electrode in the biocathode and the reference electrode in the ferrocyanide anode using the Gamry Reference 600 potentiostat.

The open circuit potential was not directly associated with light phase growth as can be seen by Figure 4.9, which shows the open circuit potential across the transition from light to dark cycle, and back to light. Only a very small change in the OCV of approximately 5 mV is seen, which indicates that either the cellular compounds which create the reductive environment take a long time to be depleted or are created in the dark phase of growth.

Increased $CO_2$ concentrations, from atmospheric to 8%, caused increased open circuit potentials but this is associated with increased growth rate and therefore higher cell concentrations rather than the $CO_2$ itself.

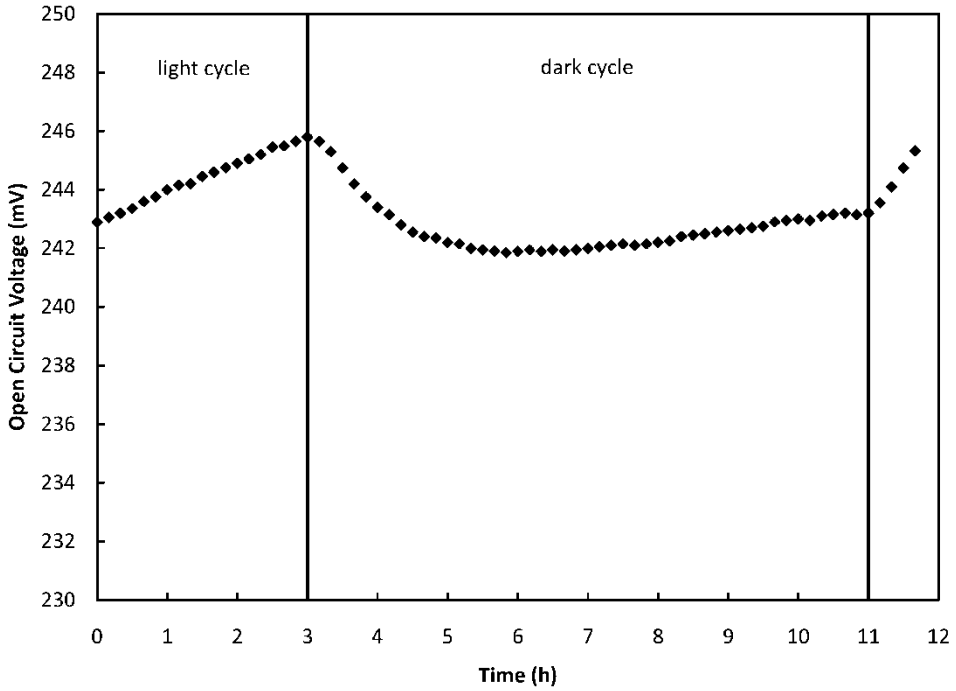


**Figure 4.9. Open circuit voltage of *C. vulgaris* cathode microbial fuel cell across the transition from light to dark and dark to light cycles. A voltage drop of approximately 5 mV is seen when switching to the dark cycle.**

The reproducibility of the steady state open circuit potential was acceptable. Among 4 experiments done with supplemental $CO_2$, the open circuit voltage varied between 0.17 V and 0.24 V (0.17, 0.20, 0.24, and 0.24).

### 4.2.3 $CO_2$ Effect

Most *Chlorella* species can only utilize dissolved $CO_2$ in its native form and not in the $HCO_3^-$ or $CO_3^{2-}$ forms (Borowitzka, 1988). This favours lower pH values since OH- ions are

being removed in going from the $HCO_3^-$ to the $CO_2$ form; more than 50% of the total dissolved carbonate is in the $CO_2$ form below a pH of 6.3, the first pKa for carbonic acid. Powell et al. reported that *Chlorella vulgaris* grows well everywhere between 5 and 7 pH. A graph showing the proportions of each carbonate form as a function of pH is shown in Figure 4.10. Lower pH values also lower the probability of bacterial contamination.

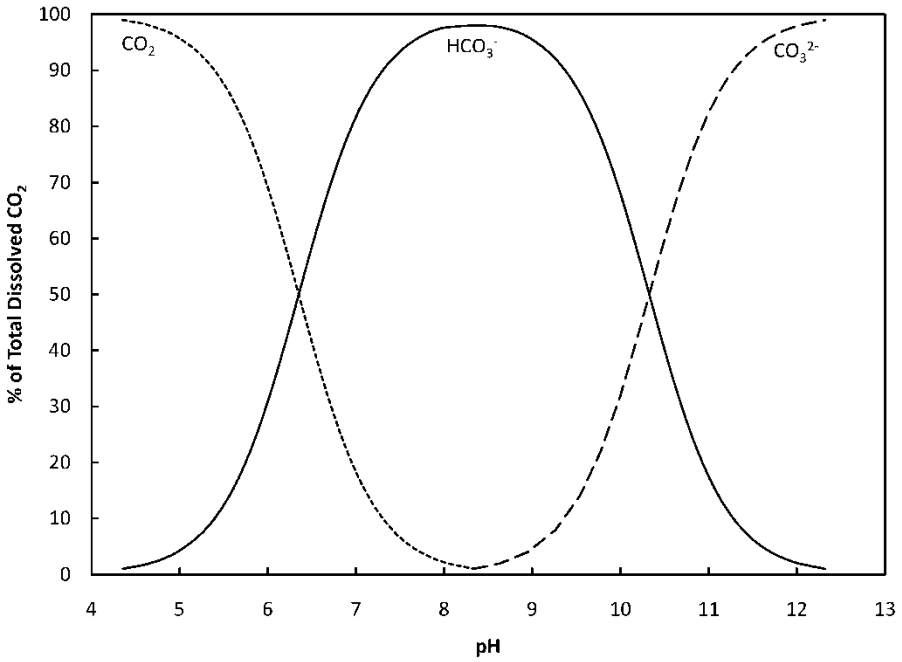


**Figure 4.10. Distribution of carbonate forms from dissolved $CO_2$ as a function of pH calculated by the Henderson–Hasselbalch equation with $pK_a$ values of 6.33 and 10.33**

Since the addition of 8% $CO_2$ tends to lower the pH below 5, the solution was maintained at 5 by addition of small amounts of sodium bicarbonate.

### 4.2.4 Transient responses to step changes

The transient response time of the microbial fuel cell was measured using potential steps at different cell voltages. Step times of four hours were used to determine response times and set up a model to determine the time taken to reach 95% of the final (4 hour) steady state. An example of the step change is shown in Figure 4.11. For this case, the step is from 370 mV

(open circuit) to 270 mV. The initial current is 26 µA and the final current is 1.09 µA. Therefore, the 95% of steady state is the time at which the current reaches 2.34 µA ((1-0.95)*(26-1.09)+1.09), which in this case is 1090 s.

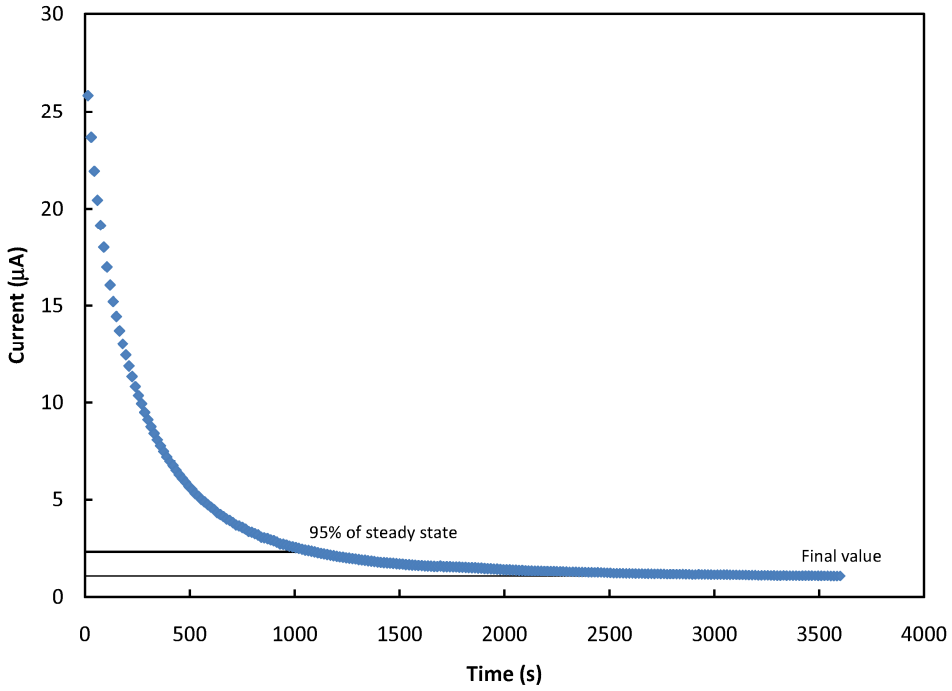


**Figure 4.11. Response to a step change in voltage of biocathode/bioanode MFC with composite pPy/Poly(MB) anode and cathode electrodes. Voltage was stepped from open circuit (approximately 370 mV) to 270 mV.**

These were done at difference cell voltages to determine the step time required for a complete polarization curve where the final current at each step is 95% of its steady state value. An example of this is shown in Figure 4.12. Each curve is consistent enough (with faster response times at lower voltages) to calculate the polarization curve with a relatively high degree of certainty (see section 4.2.7 for experimental uncertainty). The response times for 95% of steady state achieved here were all between 1800 and 3600. Fitting the data to typical first and second order response models was attempted, but the fit was not optimal and the data had very little scatter so model fitting was found to not be necessary.

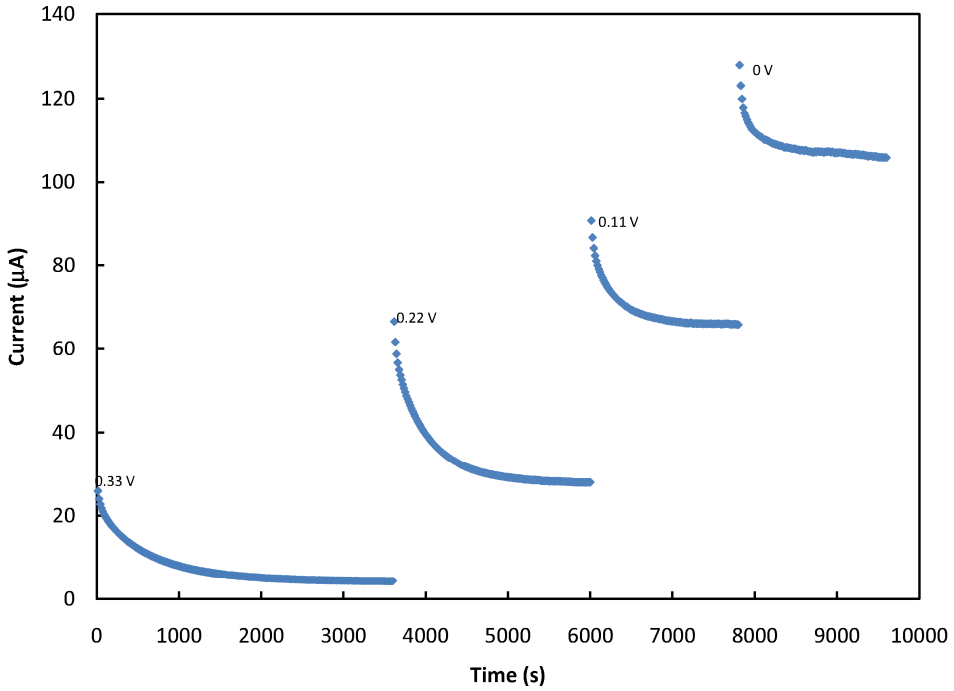


**Figure 4.12. Transient view of polarization (voltage-current measurement) tests with bioanode and biocathode. Each voltage step is held for a duration determined to give 95% of the steady state current.**

The response times observed here are much longer than reported previously using soluble mediators. Mitra et al. (2010) got response times with a *C. vulgaris* cathode of between 750 and 5000 seconds. The lower average response time is most likely due to the ability of the immobilized mediator on the electrode to store charge and its slow rate of charge transport through the polymer layer. Conversely, the soluble mediator only needs to come in contact with the graphite electrode for charge transfer to take place.

### 4.2.5 Measuring Voltage-Current Relationships and Performance

Comparisons were done between three types of electrodes in the algae biocathode with a chemical anode shown in Figure 4.13. Current density is calculated by dividing current by the geometric surface area of the electrode immersed in water. The bare graphite electrode with no mediator, as expected, allowed almost no current generation, at less than 1 $mA/m^2$ short circuit

current. Graphite with polymerized mediator showed much better results with a short circuit current of 8 mA/m$^2$ (the x intercept on voltage-current curves). The composite immobilized mediator electrode on stainless steel showed an even higher short circuit current at 65 mA/m$^2$. Powell et al. (2009) were able to get a short circuit current of approximately 24 mA/m$^2$ with soluble mediators in a similar setup. Attempts to reproduce this result were not successful.

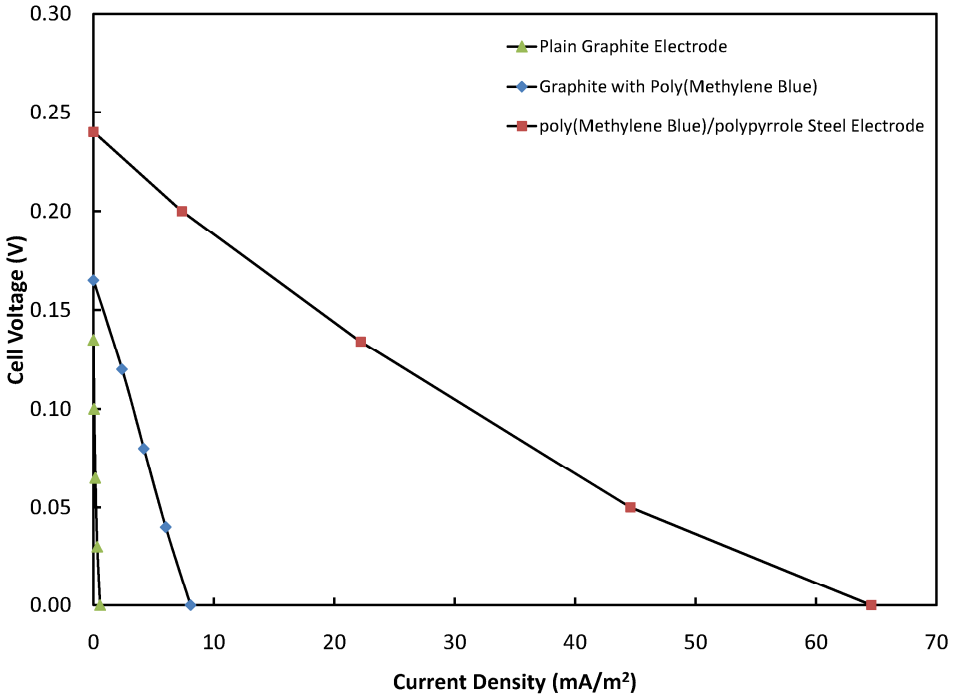


**Figure 4.13. Polarization curve with bio-cathode and chemical anode with different cathodic electrodes being compared.**

The method used to construct polarization curves was to set the potential to certain values until the current had reached 95% of steady state determined by fitting process response equations to the curve as explained in the previous section. The steady state current is recorded for each potential between the OCP and the short circuit which is then converted to a current density before being plotted as in the previous figure.

### 4.2.6 Comparisons to other values in literature

Two other research groups have developed microbial fuel cells with photosynthetic biocathodes (Powell, 2009; Cao, 2009). Since these are the most similar to the system being studied in this work, their performance was compared to that of the MFC being presented here. The following table shows some of the performance characteristics measured or calculated from those papers compared to the present work as well as one result from an aerobic (oxygen reducing) cathode (Bergel, 2005).

**Table 4.4. Performance of different types of biocathodes reported in literature.**

| | Complete MFCs | | | Chemical Anodes | | Aerobic Cathode |
|---|---|---|---|---|---|---|
| Comparison Parameter | **Present** | Cao, 2009 | Powell, 2011 | **Present** | Powell, 2009 | Bergel, 2005 |
| Open Circuit Voltage (V) | **0.37±0.05** | 0.7 | 0.27 | **0.21±0.04** | 0.07 | 0.2 (vs.SCE) |
| Power Density (mA/m$^2$) | **7±2** | 750* | 1 | **0.7±0.1** | - | 270 |

*not directly comparable because true surface area was not used (geometric surface area of graphite felt)

As can be seen here, the maximum power density, current density, and open circuit voltage are lower than in aerobic biocathodes or cathodes using photosynthetic bacteria, but higher than using *Chlorella vulgaris* with soluble mediators.

### 4.2.7 Measuring experimental uncertainty in polarization curves

Uncertainty was measured by repeating the same polarization curve measurement on different days with different electrodes, since experiments with different electrodes are being compared. The average of three measurements was taken and plotted with error bars used to represent the maximum and minimum of the three measurements in Figure 4.14.

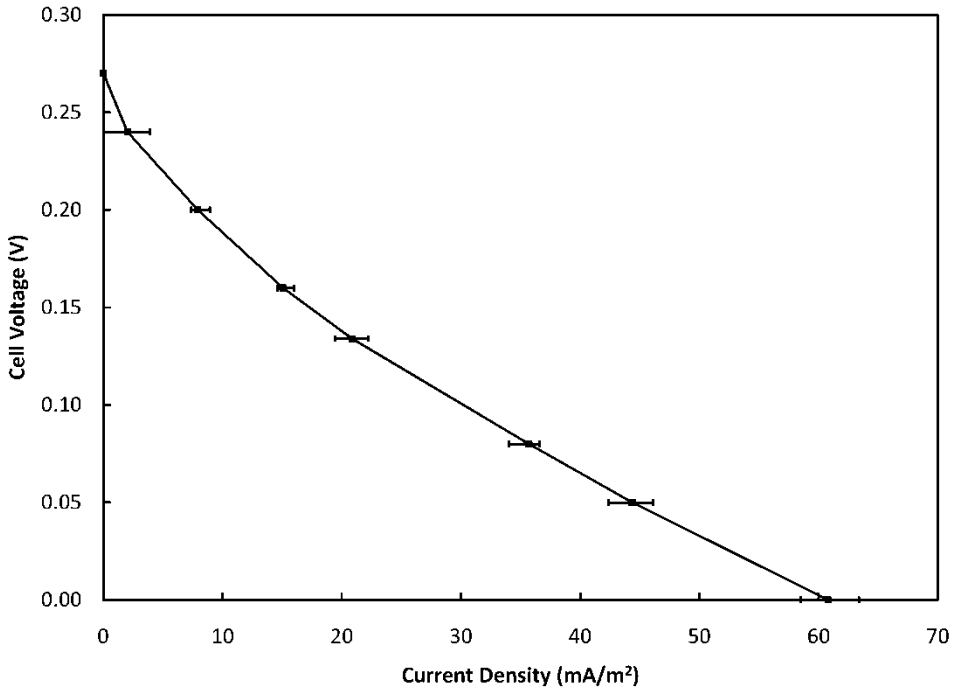


**Figure 4.14. Polarization curve with bioanode (soluble mediator) with error bars. Data points are the average of three separate polarization curves on consecutive days and the bars are the range of the three measurements.**

A second method was also used to calculate the variance in the current measurements during polarization curve measurements. Samples were taken all at different times and different days. A total of 14 sample points were used to calculate variance. The standard error of the sample was calculated using equation 4.1.

$$s = \sqrt{\frac{1}{N-1}\sum_{i=1}^{N}(x_i - \bar{x})^2} \qquad (4.1)$$

Where in this case, N is the number of samples (14), x are the current measurements, and s is the sample standard deviation. The standard deviation for the current during biocathode measurements was found to be 1.8 mA/m$^2$.

Uncertainty was also gauged by looking at the variation in the open circuit potentials of the biocathode microbial fuel cell. As seen in section 4.2.2, the voltages were in the range of 0.17 to

0.24 V. The samples using the coupled bioanode and biocathode microbial fuel cell had all five experiments showing an open circuit voltage between 0.27 V and 0.37 V as discussed in section 4.3.

The likely causes of experimental variation are the different growth patterns of the biomass and the bio-fouling of the membrane with cells. Additionally, the immobilized mediator electrodes showed some variability due to slight differences in the steel surface, electrode placement, and ageing of the pyrrole.

## 4.3 Microbial Fuel Cell with Coupled Bioanode and Biocathode

A coupled microbial fuel cell with bioanode and biocathode was operated and examined with different electrode types, surface areas, and cathode volumes. Figure 4.15 shows the voltage, current, and power characteristics of a microbial fuel cell with *Saccharomyces cerevisiae* in the anode and *Chlorella vulgaris* in the cathode (used for all further experiments). For that first experiment, a composite immobilized mediator steel electrode (polypyrrole and poly(mehthylene blue) on 304L stainless steel) was used in the cathode and a graphite electrode with soluble mediator was used in the anode. This shows a much larger maximum current and power density than achieved with any other electrode configuration and similar volumes including using a soluble mediator in both chambers reported by Powell et al. (2011). Figure 4.15 shows the power density normalized to the surface area of one electrode and cell voltage both as a function of current density for this setup. Both electrodes were immersed 6 cm into the solution and had an exposed surface area of 11.3 $cm^2$.

The error bars show the relative standard deviation of current measurements between different polarization curves run on the same setup. Values of standard deviation were

calculated previously and applied to each of the following figures by normalizing the standard deviation based on the magnitude of the short circuit current.

The open circuit potentials of the completely biological cell were also reasonably reproducible, with the 5 separate experimental runs (in which polarization curves were obtained) showed open circuit cell voltages between 0.27 V and 0.37 V.

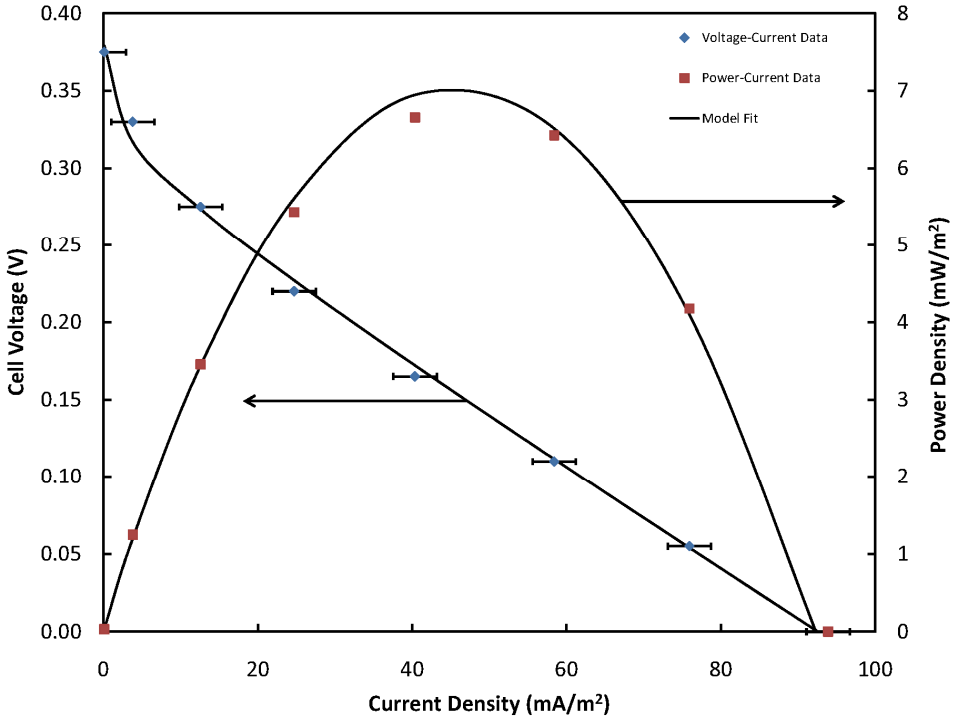


**Figure 4.15. Polarization and power curves for bioanode/biocathode microbial fuel cell with soluble mediator graphite anode and immobilized mediator steel cathode along with fit to basic model. Error bars show the relative standard deviation of current measurements.**

The anodes were also tested with immobilized mediator steel electrodes. The same electrodes were used in the anode and cathode. The resulting voltage, current, and power relationships are shown in Figure 4.16. Immobilized mediators have not been shown to be effective previously with yeast anodes though there is some discrepancy between different authors regarding the role of mediators in such systems (Liu, 2010).

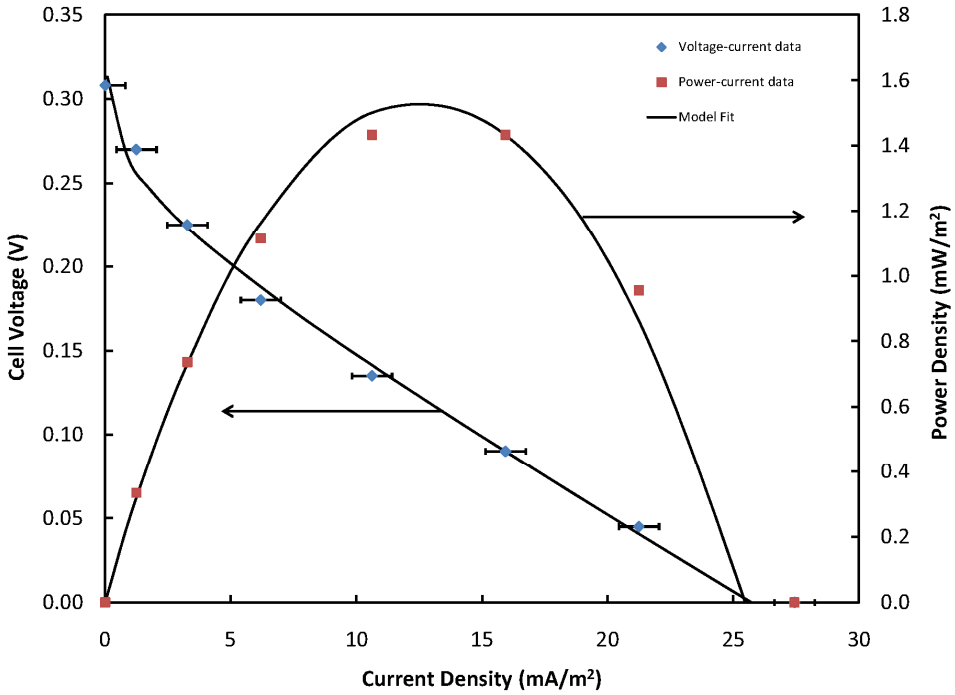


**Figure 4.16. Polarization and power curves for microbial fuel cell with bioanode and biocathode each with an immobilized mediator steel electrode. Electrochemical resistance model fit lines shown. Error bars show the relative standard deviation of current measurements.**

It can be seen that the use of these immobilized mediators drastically decreases the power and current produced when used in the anode. Maximum power is decreased by a factor of 4.5 and short circuit current by a factor of 3.5. Open circuit potential (y intercept) is slightly lower with the immobilized mediator anode but not significantly so.

### 4.3.1 Open Circuit Voltages of Coupled MFC

The open circuit potentials of the MFC with biocathode and bioanode increased with time as the biomass concentration increased and as the biofilm formed on the electrode. Figure 4.17 shows the increase of open circuit potential of the MFC as the cells begin to interact with the electrode. This shows that the open circuit potential, not just the current generation, is limited by the cell concentration and development of the biofilm.

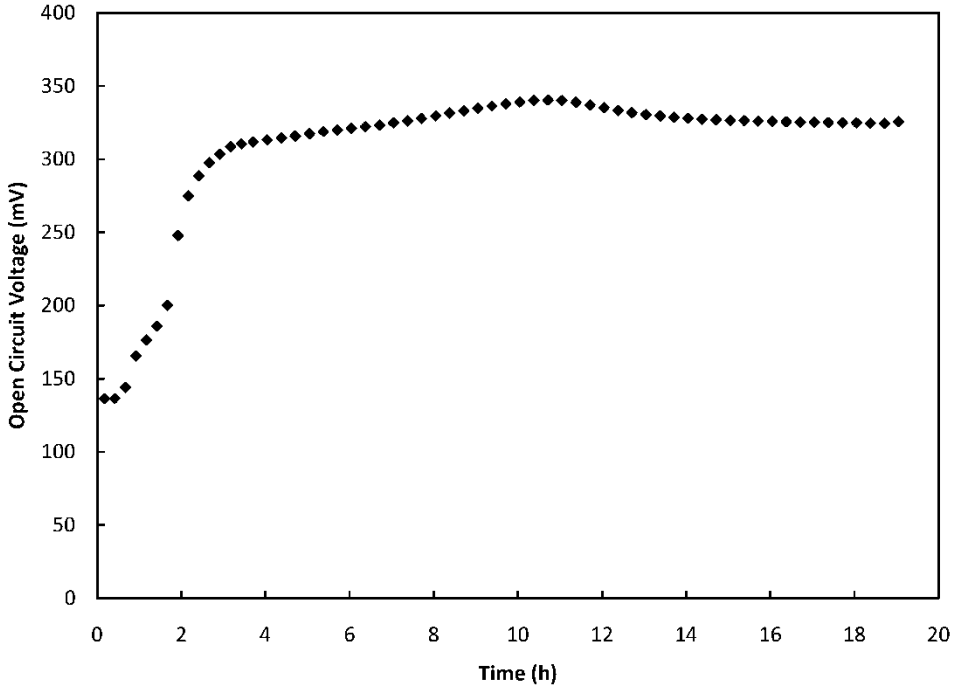


**Figure 4.17. Evolution of the open circuit voltage of a biocathode/bioanode microbial fuel cell after inoculation with a starter culture of *C. vulgaris* in the cathode and a dry culture of *S. cerevisiae* in the anode.**

### 4.3.2 Summary of Different Electrodes Used in the MFC

The primary electrodes being tested are the composite immobilized mediator electrodes which, as described in the previous chapters, are based on 304L stainless steel with layers of polypyrrole and poly(methylene blue) deposited on them. These electrodes were compared to graphite electrodes with soluble mediators in the yeast bioanodes and, in addition to these, with no mediator and immobilized mediator on graphite in algae biocathodes.

### 4.3.3 Model Fitting to Polarization Curve Data

A one dimensional physical model was previously proposed to model the processes in the MFC with partial differential equations but it was found to have too many flaws to be justifiably applied to such a system and many of the parameters would not have been obtainable. Instead,

in order to show fit lines on the polarization and power (power density versus current density) curves, a simple electrochemical resistance model used for chemical fuel cells was used without the mass transfer term, shown in equation 4.2 (O'Hayre, 2006) and explained further in Chapter 2.

$$E = E° - (a + b\ lni) - R_{\Omega} i \qquad (4.2)$$

E is the cell potential, $E_0$ is the equilibrium potential, 'a' and 'b' are terms for the activation resistance, while 'i' is the current density. Examples of this fit being used are shown in Figure 4.15 and Figure 4.16. The mass transfer term has been eliminated as there is no indication of mass transfer limitation in this or other similar microbial fuel cells.

### 4.3.4 Evaluation of Anode and Cathode using Reference Electrodes

The relative impact of the anode and cathode on the overall internal resistance can be determined by placing a reference electrode in the cell and recording the polarization curve while simultaneously measuring the voltage between the anode electrode and the reference electrode with a multimeter. The voltage of the cathode with respect to the reference is then determined by subtracting the anode potential (with respect to the reference) from the overall cell voltage at each current.

Figure 4.18 shows a polarization curve with the voltage current relationships plotted separately for the anode and cathode. Each is reported with respect to the reference electrode. The cathode shows more of an activation overpotential since the slope of the line is higher near the zero-current intercept than the rest of the curve.

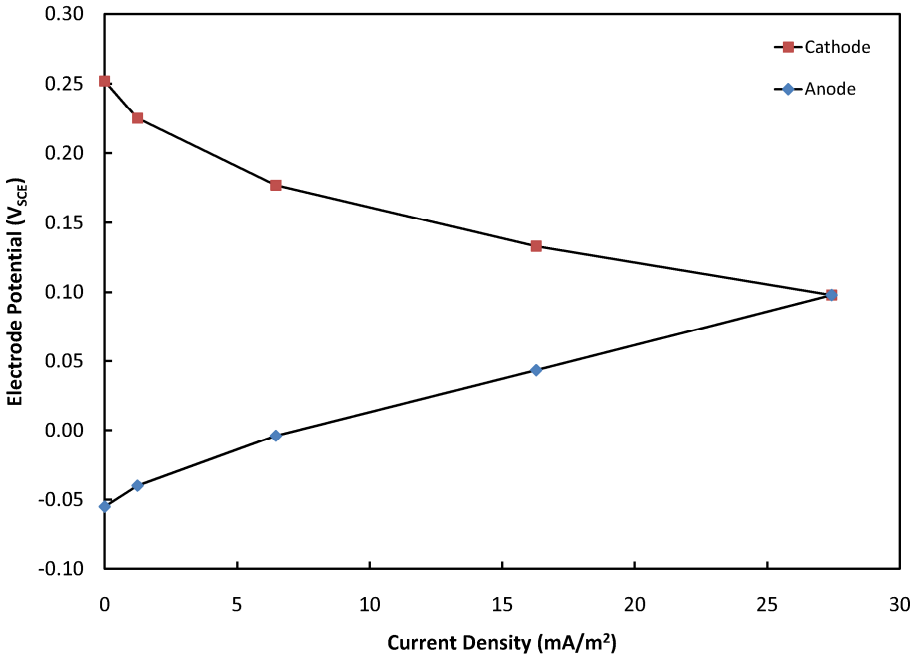


**Figure 4.18. Polarization curves showing the potentials of the anode and cathode separately. A reference electrode is placed in the anode and voltages are taken between each electrode and the reference. The cathode curve will include electrolyte resistance in this figure.**

If the reference electrode is placed in the anode, as shown in Figure 4.18, the cathode voltage curve will include the voltage drop due to the membrane and electrolyte resistance. Conversely, the reference electrode can be placed in the cathode and the reverse will be true. In order to separate the impact of the membrane from that of the anode and cathode, two reference electrodes can be used.

### 4.3.5 Internal Resistance Components

Through the use of reference electrodes and multiple simultaneous potential measurements, it is possible to determine several different components of the internal resistance of a microbial fuel cell. While some authors (Bretschger, 2010) have used a single reference electrode in the anode or cathode and measured the potential-current relationships of each chamber this way, as in the previous section of this report, more useful information can be obtained with a reference

electrode in each chamber. The potential of the anode with respect to a reference in the anode chamber gives the polarization characteristics of the anode alone. The same holds for a reference electrode in the cathode. The remaining potential (measured either across the two references or by subtracting the potentials of the anode and cathode from the overall cell potential) is the membrane or liquid junction potential and, when current is flowing, the voltage loss due to ohmic resistances. The membrane or liquid junction potential is due to the difference in the mobility of ions on either side of the membrane and the difference in pH. Ohmic resistances exist primarily across the membrane itself but also to a smaller extent in the anode and cathode solutions depending on their ionic concentrations. The effect on the overall resistances in the microbial fuel cell of each component is shown in Figure 4.19. Voltages are with respect to the short circuit point so the slope of each line represents the internal resistance of that component.

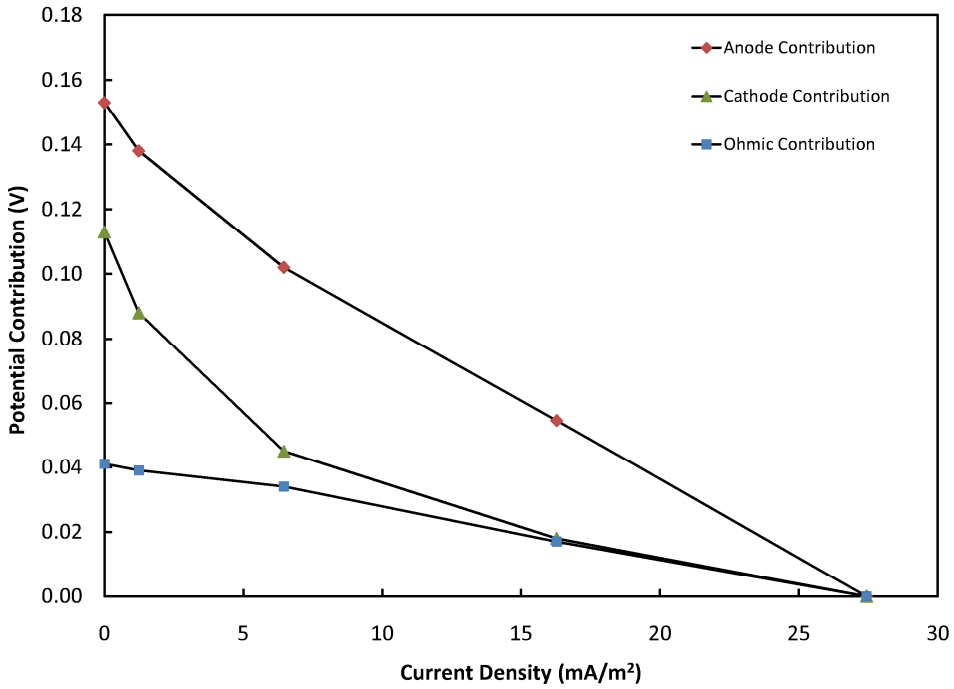


**Figure 4.19. Resistance of anode, cathode, and electrolyte with bio-anode and bio-cathode with immobilized mediator electrodes used for each. The negative slope of each line corresponds to the internal resistance of the given component at that current.**

Further, a graph showing the potential across the membrane at different currents shows a linear slope indicating change in voltage due to the ohmic resistance and the membrane or liquid junction potential (Figure 4.20). Liquid junction potentials are due to different mobilities of anions and cations across a membrane or other liquid junction. The primary membrane potential here, however, is due to the difference in pH across the membrane. The effect of this difference in pH can be calculated using the Nernst equation. Given the pH of 4.1 in the anode and an average pH of 5 in the cathode, this contributes -53 mV to the membrane potential (see Appendix A for calculation).

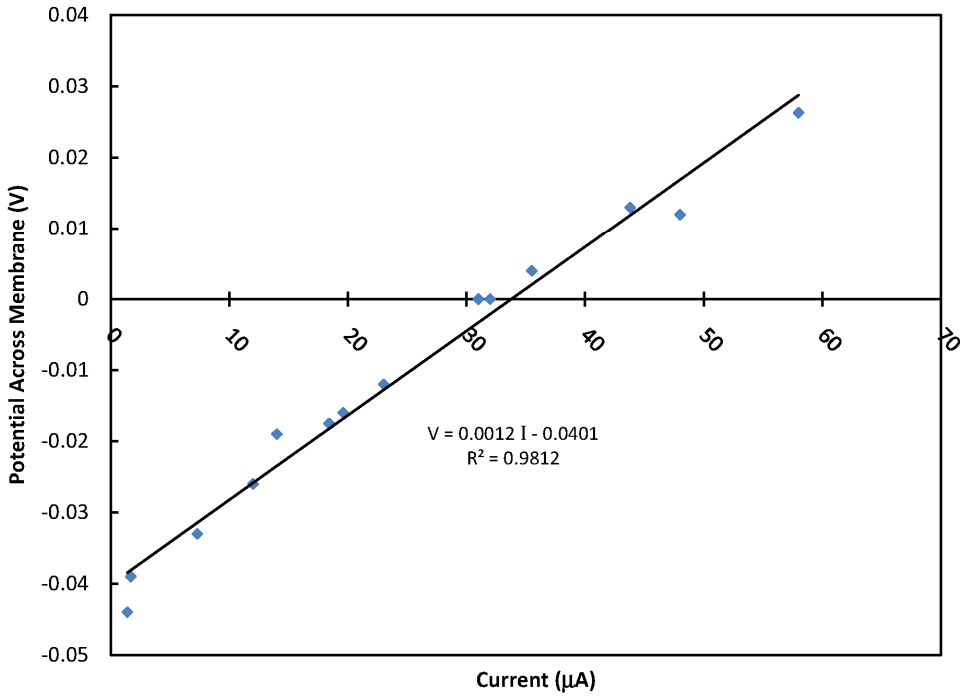


**Figure 4.20. Plot of voltage across the membrane and electrolyte in the MFC and a best fit line. Liquid junction (membrane) potential is shown at the zero current intercept and the slope represents the iR drop due to the ohmic resistance in the solution and the membrane.**

Since the y-intercept (zero current membrane potential) is -40 mV, 13 mV can be attributed to liquid junction potentials and experimental error.

# 5. CONCLUSIONS AND RECOMMENDATIONS

## 5.1 Conclusions

Creating stable, immobilized electron transfer mediators which are biocompatible presents a significant challenge. Electrically conductive polypyrrole coatings have been deposited on stainless steel 304L with several different doping ions. The coatings with salicylate ions were found to be stable in aqueous solutions for use in microbial fuel cells. Methylene blue, which has been shown to mediate electron transfer with living cells and immobilized enzymes, was polymerized on polypyrrole coated steel. These composite coatings were shown to facilitate the oxidation of NADH by cyclic voltammetry. These composite coatings were studied using electrochemical impedance spectroscopy and found to have much lower charge transfer resistances than polypyrrole alone indicating they could be suitable for microbial fuel cells.

A microbial fuel cell with a photosynthetic biocathode using $CO_2$ as the electron acceptor has been operated successfully with several different electrode/mediator combinations. The cathode relied on the microalgae *Chlorella vulgaris* for photosynthesis. The composite polypyrrole/poly(methylene blue) mediators were found to offer higher electrical performance in these biocathodes than soluble mediators, immobilized mediators on graphite, and mediatorless systems.

A completely biological fuel cell was operated with a bioanode based on *Saccharomyces cerevisiae* metabolizing glucose along with the aforementioned biocathode. The performance of the bioanode with the composite immobilized mediator was found to be lower than when using

soluble mediators in combination with graphite electrodes. This indicates that interaction between the yeast cells and the electrode is limited when the mediator is unable to fully diffuse into the cells. The complete bioanode/biocathode MFC had better performance than previous systems when a soluble mediator anode was combined with an immobilized mediator cathode with power density increased by a factor of 7 compared to a soluble mediator system.

Growth rates were not found to be significantly affected by microbial fuel cell operation, although when soluble mediators are used, the growth rate of the algae is decreased due to blockage of the light.

## 5.2 Recommendations

There is a large knowledge gap remaining regarding biocathodes in general but specifically with photosynthetic cathodes. In the case of bioanodes, mechanisms of electron transfer from cells to electrodes have been studied by cyclic voltammetry among other techniques, whereas this has not been determined for photosynthetic cathodes. Likewise, while many different types of bacteria and fungi have been found to generate an anodic current with or without mediators, very few photosynthetic species have been studied for this purpose. Other species of cyanobacteria and microalgae should be examined for cathodic current generation both with immobilized mediator electrodes and in the absence of mediators. Species which do not require electron mediators could be studied by CV when grown as a biofilm to determine charge transfer mechanisms.

The effect of microbial fuel cell operation on growth and morphology, specifically with these immobilized mediator electrodes, should be examined using more more frequent biomass concentration measurements. The impact of the biomass on power generation could be

examined by doing experiments with the biomass filtered out of the solution and with no biomass present.

Since the composite mediator electrodes were found to perform better than soluble mediators in photosynthetic biocathodes, they should be tested in bioanodes using different bacteria with different cell membrane proteins as well as the effect on growth of microbial fuel cell operation and any toxic effects of the electrode.

Cell and electrode geometry optimization was not attempted. Performance and economics of these MFCs would be greatly increased with high surface area electrodes and optimized membrane/bridge geometries. Parallel flat plate electrodes and steel wool/mesh are two promising electrode geometries requiring further investigation. Beyond the basic surface area to volume and weight ratios, issues regarding flow and mass transfer limitations could then become issues worthy of investigation as well.

Although polypyrrole has been shown to be biocompatible and give desirable surface characteristics, other conductive coatings could be investigated to support the actual mediator layer. In this research, however, the performance with mediator on bare graphite was rather disappointing indicating a synergistic effect between the polypyrrole and methylene blue layers.

# REFERENCES


Bard, A.J., and L.R. Faulkner, *Electrochemical Methods, Fundamentals and Applications*, 2nd Ed., Wiley, New York (2000).

Bergel, A., D. Féron, and A. Mollica, Catalysis of oxygen reduction in PEM fuel cell by seawater biofilm, *Electrochem. Comm.* **7**, 900–904 (2005).

Borowitzka, M. A., L. J. Borowitzka, *Micro-algal biotechnology*, Cambridge University Press, Cambridge (1988).

Bretschger, O., A.C.M. Cheung, F. Mansfeld, and K.H. Nealson, Comparative Microbial Fuel Cell Evaluations of *Shewanella* spp., *Electroanal.* **22**, 883–894 (2010).

Cao, X., X. Huang, P. Liang, N. Boon, M. Fan, L. Zhang, and Z. Zhang, A completely anoxic microbial fuel cell using a photo-biocathode for cathodic carbon dioxide reduction, *Energy Environ. Sci.* **2**, 498–501 (2009).

Chi, Q. and S. Dong, Electrocatalytic oxidation of reduced nicotinamide coenzymes at Methylene Green-modified electrodes and fabrication of amperometric alcohol biosensors, *Anal. Chim. Acta* **285**, 125–133 (1994).

Dumas, C., A. Mollica, D. Féron, R. Basséguy, L. Etcheverry, A. Bergel, Marine microbial fuel cell: Use of stainless steel electrodes as anode and cathode materials, *Electrochim. Acta.* **53**. 468–473 (2007).

Fan, Y., E. Sharbrough, and H. Liu, Quantification of the Internal Resistance Distribution of Microbial Fuel Cells, *Environ. Sci. Technol.* **42**, 8101–8107 (2008).

Feng, C., L. Ma, F. Li, H. Mai, X. Liang, and S. Fan, A polypyrrole/anthraquinone-2,6-disulphonic disodium salt (PPy/AQDS)-modified anode to improve performance of microbial fuel cells, *Biosens. Bioelectron.* **25**, 1516–1520 (2010).

Ferloni, P., M. Mastragostino, and L. Meneghello, Impedance analysis of electronically conducting polymers, *Electrochim. Acta* **41**, 27–33 (1996).

Fricke, K., F. Harnisch and U. Schröder, On the use of cyclic voltammetry for the study of anodic electron transfer in microbial fuel cells, *Energy Environ. Sci.* **1**. 144–147 (2008).

Ganguli, R. and B. S. Dunn, Kinetics of Anode Reactions for a Yeast-Catalysed Microbial Fuel Cell**,** *Fuel Cells* **9**, 44–52 (2008).

Gros P. and M. Comtat, A bioelectrochemical polypyrrole-containing $Fe(CN)_6^{3-}$ interface for the design of a NAD-dependent reagentless biosensor, *Biosens. Bioelectron.* **20**, 204–210 (2004).

Heijne, H. V. M., Hamelers, M. Saakes, and C. J. N. Buisman, Performance of non-porous graphite and titanium-based anodes in microbial fuel cells, *Electrochim. Acta* **53**, 5697–5703 (2008).

James, D. E., Algae Media, *Culturing Algae*, Carolina Biological Supply Company, Burlington (1978).

Ju, H., J. Zhou, C. Cai, and H. Chen, The Electrochemical Behavior of Methylene Blue at a Microcylinder Carbon Fiber Electrode, *Electroanal.* **7**. 1165–1170 (1995).

Karyakin, A. A., E. E. Karyakina, and H. L. Schmidt, Electropolymerized azines: a new group of electroactive polymers, *Electroanal.* **11**, 149–155 (1999).

Liu, Y., W. Li, X. Hu, and Y. Yin, The study of mediator-less microbial fuel cell based on saccharomyces cerevisiae, *Mechatron. Embedded Sys. and Appl.* 361–363 (2010).

Logan, B. E., Exoelectrogenic bacteria that power microbial fuel cells, *Nature Rev. Microbiol.* **7**, 375 – 381 (2009).

Logan, B. E., S. Cheng, V. Watson, and G. Estadt, Graphite Fiber Brush Anodes for Increased Power Production in Air-Cathode Microbial Fuel Cells, *Environ. Sci. Technol.* **41**, 3341–3346 (2007).

Logan, B.E., B. Hamelers, R. Rozendal, U. Schröder, J. Keller, S. Freguia, P. Aelterman, W. Verstraete, and K. Rabaey, Microbial Fuel Cells: Methodology and Technology, *Environ. Sci. Technol.* **40**, 5181–5192 (2006).

Manohar, A.K., O. Bretschger, K.H. Nealson, and F. Mansfeld, The use of electrochemical impedance spectroscopy (EIS) in the evaluation of the electrochemical properties of a microbial fuel cell, *Bioelectrochem.* **72**, 149–154 (2008).

Manohar, A.K. and F. Mansfeld, The internal resistance of a microbial fuel cell and its dependence on cell design and operating conditions, *Electrochim. Acta* **54**, 1664–1670 (2009).

Marcus, A.K., C.I. Torres, and B.E. Rittmann, Conduction-Based Modeling of the Biofilm Anode of a Microbial Fuel Cell, *Biotechnol. Bioeng.* **98**, 1171–1182 (2007).

Marsili, E., J.B. Rollefson, D.B. Baron, and R.M. Hozalski, D.R. Bond, Microbial Biofilm Voltammetry: Direct Electrochemical Characterization of Catalytic Electrode-Attached Biofilms, *Appl. Environ. Microbiol.* **74**, 7329–7337 (2008).

Martins, J. I., T.C. Reis, M. Bazzaoui, E. A. Bazzaoui, and L. Martins, Polypyrrole coatings as a treatment for zinc-coated steel surfaces against corrosion, *Corros. Sci.* **46**. 2361–2381 (2004).

Mitra, P., A. Vigueras, G. Hill, Enhanced photosynthetic growth, biodiesel and electricity production using *C. vulgaris* and *P. pudita* / *S. Cerevisiae*, *$CO_2$ Summit: Technology & Opportunity*, Vail, CO (2010).

Morozan, A., I. Stamatin, L. Stamatin, A. Dumitru, K. Scott, Carbon electrodes for microbial fuel cells, *J. Optoelectron. Adv. Mater*. **9**, 221–224 (2007).

O'Hayre, R., S-W. Cha, W. Colella, F. B. Prinz, *Fuel Cell Fundamentals*, Wiley & Sons, New York (2006).

Orazem, M. E., B. Tribollet, *Electrochemical Impedance Spectroscopy*. Wiley-Interscience, New York (2008).

Park, D.H., J.G. Zeikus, Improved Fuel Cell and Electrode Designs for Producing Electricity from Microbial Degradation, *Biotechnol. Bioeng.* **81**, 348–355 (2003).

J. Petitjean, S. Aeiyach, J. C. Lacroix, and P. C. Lacaze, Ultra-fast electropolymerization of pyrrole in aqueous media on oxidizable metals in a one-step process, *J. Electroanal. Chem.* **478**, 92–100 (1999).

Picioreanu, C., I.M. Head, K.P. Katuri, M.C.M. van Loosdrecht, K. Scott, A computational model for biofilm-based microbial fuel cells, *Water Res.* **41**, 2921–2940 (2007).

Picioreanu, C., K.P. Katuri, I.M. Head, M.C.M. van Loosdrecht, K. Scott, Mathematical model for microbial fuel cells with anodic biofilms and anaerobic digestion, *Water Sci. Technol.* **57**, 965–971 (2008).

Powell, E.E., M.L. Mapiour, R.W. Evitts, G.A. Hill, Growth kinetics of Chlorella vulgaris and its use as a cathodic half cell, *Biores. Technol.* **100**, 269–274 (2009).

Powell, E.E., J.C. Bolster, G.A. Hill, and R.W. Evitts, Microbial Fuel Cell with a Photosynthetic Microalgae Cathodic Half Cell Coupled to a Yeast Anodic Half Cell, *Energy Sources Part A* **33**, 440–448 (2011).

Prieto-Simón, B. and E. Fàbregas, Comparative study of electron mediators used in the electrochemical oxidation of NADH, *Biosens. Bioelectron.* **19**, 1131–1138 (2004).

Qiao, Y., C.M. Li, S-J. Bao, Q-L. Bao, Carbon nanotube/polyaniline composite as anode material for microbial fuel cells, *J. Power Sources* **170**, 79–84 (2007).

Rosenbaum, M., F. Zhao, U. Schröder, F. Scholz, Interfacing Electrocatalysis and Biocatalysis with Tungsten Carbide: A High-Performance, Noble-Metal-Free Microbial Fuel Cell, *Angew. Chem*. **118**, 1–4 (2006).

Schirmeisen, M. and F. Beck, Electrocoating of iron and other metals with polypyrrole, *J. Appl. Electrochem.* **19**, 401–409 (1989).

Schröder, U., Anodic electron transfer mechanisms in microbial fuel cells and their energy efficiency, *Phys. Chem. Chem. Phys.* **9**, 2619–2629 (2007).

Schröder, U., J. Nießen, F. Scholz, A Generation of Microbial Fuel Cells with Current Outputs Boosted by More Than One Order of Magnitude, *Angew. Chem.* **115**, 2986–2989 (2003).

Schuhmann, W., J. Huber, H. Wohlschläger, B. Strehlitz, and B. Gründig, Electrocatalytic oxidation of NADH at mediator-modified electrode surfaces, *J. Biotechnol.* **27**, 129–142 (1993).

Scott, K., G.A. Rimbu, K.P. Katuri, K.K. Prasad, I.M. Head, Application of modified carbon anodes in microbial fuel cells, *Process Saf. Environ. Prot.* **85**, 481–488 (2007).

Silber, A., N Hampp, and W. Schuhmann, Poly (methylene blue)-modified thick-film gold electrodes for the electrocatalytic oxidation of NADH and their application in glucose biosensors, *Biosens. Bioelectron.*, **11**, 215–223 (1996).

Vernitskaya, T. V., O. N. Efimov, Polypyrrole: a conducting polymer; its synthesis, properties and applications, *Russ. Chem. Rev.* **66**, 443–457 (1997).

Wall, J. B., G. A. Hill, Optimum CFST Bioreactor Design: Experimental Study Using Batch Growth Parameters for *Saccharomyces cerevisiae* Producing Ethanol, *Can. J. Chem. Eng.* **70**. 148–152 (1992).

Wang, L. X., X. G. Li, Y. L. Yang, Preparation, properties and applications of polypyrroles, *React. Funct. Polym.* **47**, 125–139 (2001).

Zeng, Y., Y.-F. Choo, B.-H. Kim, and P. Wu, Modelling and simulation of two-chamber microbial fuel cell, *J. Power Sources.* **195**, 79–89 (2010).

Zhang, X-C. and A. Halme, Modelling of a Microbial Fuel Cell Process, *Biotechnol. Lett.* **17**, 809–814 (1995).

Zhang, T., Y. Zeng, S. Chen, X. Ai, and H. Yang, Improved performances of *E. coli*-catalyzed microbial fuel cells with composite graphite/PTFE anodes, *Electrochem. Commun*. **9**, 349–353 (2007).

# APPENDIX A. CALCULATION OF THEORETICAL POTENTIALS

## Calculation of $CO_2$/glucose reduction half cell reaction potential

Glucose half-cell reduction reaction:

$$6\ CO_2 + 12\ H^+ + 12\ e^- \rightarrow C_6H_{12}O_6\ (\text{biomass}) + 3\ O_2$$

Gibbs free energies of formation:

| | |
|---|---|
| $CO_2$ | -394.4 kJ/mol |
| $H^+$ | 0 kJ/mol |
| $e^-$ | 0 kJ/mol |
| $O_2$ | 0 kJ/mol |
| $C_6H_{12}O_6$ | -910.6 kJ/mol |

Calculation of $\Delta G°_{rxn}$ and E°

$\Delta G^0_{rxn}$ = 6 (-394.4 kJ/mol) – (-910 kJ/mol)

$\Delta G^0_{rxn}$ = -1456 kJ/mol

Calculation of E° from

$$E° = \frac{\Delta G°}{nF}$$

$$E° = \frac{-1456000\ J/mol}{(12)(96485\ C/mol)}$$

$$E° = -1.26\ V$$

## Calculation of potential across a membrane due to a pH difference

Nernst equation:

$$E = E° - \frac{RT}{nF} ln(\Pi)$$

For pH differences, $H^+$ concentrations are taken into consideration and the E° is ignored:

$$E_{pH} = -\frac{RT}{nF} ln\left(\frac{H^+_{anode}}{H^+_{cathode}}\right)$$

$$E_{pH} = -\frac{RT}{nF} log\left(\frac{H^+_{anode}}{H^+_{cathode}}\right) ln(10)$$

$$E_{pH} = -ln(10)\frac{RT}{nF}\left(log(H^+_{anode}) - \log\left(H^+_{cathode}\right)\right)$$

$$E_{pH} = -2.303\frac{(8.3145\ Jmol^{-1}K^{-1})(298\ K)}{(1)(96485\ Cmol^{-1})}(pH_{cathode} - pH_{anode})$$

$$E_{pH} = 0.0591\ \Delta pH_{(anode-cathode)}$$

For the microbial fuel cell, the pH of the anode is 0.9 lower than the cathode (4.1 and 5)

$$E_{pH} = 0.0591\ \Delta pH_{(anode-cathode)}$$

$$E_{pH} = 0.0591\ (-0.9)$$

$$E_{pH} = -0.053\ V$$